

# Open Research Online

---

The Open University's repository of research publications and other research outputs

## Long-term climate change commitment and reversibility: an EMIC intercomparison

### Journal Item

#### How to cite:

Zickfeld, Kirsten; Eby, Michael; Alexander, Kaitlin; Weaver, Andrew J.; Crespin, Elisabeth; Fichet, Thierry; Goosse, Hugues; Philippon-Berthier, Gwenaëlle; Edwards, Neil R.; Holden, Philip B.; Eliseev, Alexey V.; Mokhov, Igor I.; Feulner, Georg; Kienert, Hendrik; Perrette, Mahé; Schneider von Deimling, Thomas; Forest, Chris E.; Friedlingstein, Pierre; Joos, Fortunat; Spahni, Renato; Steinacher, Marco; Kawamiya, Michio; Tachiiri, Kaoru; Kicklighter, David; Monier, Erwan; Schlosser, Adam; Sokolov, Andrei; Matsumoto, Katsumi; Tokos, Kathy S.; Olsen, Steffen M.; Pedersen, Jens O. P.; Ridgwell, Andy; Shaffer, Gary; Yoshimori, Masakazu; Zeng, Ning and Zhao, Fang (2013). Long-term climate change commitment and reversibility: an EMIC intercomparison. *Journal of Climate*, 26(6) pp. 5782–5809.

For guidance on citations see [FAQs](#).

© 2013 American Meteorological Society

Version: Accepted Manuscript

Link(s) to article on publisher's website:  
<http://dx.doi.org/doi:10.1175/JCLI-D-12-00584.1>

---

Copyright and Moral Rights for the articles on this site are retained by the individual authors and/or other copyright owners. For more information on Open Research Online's data [policy](#) on reuse of materials please consult the policies page.

---



# AMERICAN METEOROLOGICAL SOCIETY

*Journal of Climate*

## **EARLY ONLINE RELEASE**

This is a preliminary PDF of the author-produced manuscript that has been peer-reviewed and accepted for publication. Since it is being posted so soon after acceptance, it has not yet been copyedited, formatted, or processed by AMS Publications. This preliminary version of the manuscript may be downloaded, distributed, and cited, but please be aware that there will be visual differences and possibly some content differences between this version and the final published version.

The DOI for this manuscript is doi: 10.1175/JCLI-D-12-00584.1

The final published version of this manuscript will replace the preliminary version at the above DOI once it is available.

If you would like to cite this EOR in a separate work, please use the following full citation:

Zickfeld, K., M. Eby, K. Alexander, A. Weaver, E. Cressin, T. Fichefet, H. Goosse, G. Philippon-Berthier, N. Edwards, P. Holden, A. Eliseev, I. Mokhov, G. Feulner, H. Kienert, M. Perrette, T. Schneider von Deimling, C. Forest, P. Friedlingstein, F. Joos, R. Spahni, M. Steinacher, M. Kawamiya, K. Tachiiri, D. Kicklighter, E. Monier, A. Schlosser, A. Sokolov, K. Matsumoto, K. Tokos, S. Olsen, J. Pedersen, A. Ridgwell, G. Shaffer, M. Yoshimori, N. Zeng, and F. Zhao, 2013: Long-term Climate Change Commitment and Reversibility: An EMIC Intercomparison. *J. Climate*. doi:10.1175/JCLI-D-12-00584.1, in press.



1 **Long-term Climate Change Commitment and Reversibility: An**

2 **EMIC Intercomparison**

3 **KIRSTEN ZICKFELD \***

*Department of Geography, Simon Fraser University, Burnaby, BC, Canada*

4 **MICHAEL EBY, KAITLIN ALEXANDER, ANDREW J. WEAVER**

*School of Earth and Ocean Sciences, University of Victoria, Victoria, BC, Canada*

5 **ELISABETH CRESPIN, THIERRY FICHEFET, HUGUES GOOSSE**

**GWENAËLLE PHILIPPON-BERTHIER**

*Université Catholique de Louvain, Earth and Life Institute,*

*Georges Lemaître Centre for Earth and Climate Research, Louvain-La-Neuve, Belgium*

6 **NEIL R. EDWARDS, PHILIP B. HOLDEN**

*The Open University, Milton Keynes, United Kingdom*

7 **ALEXEY V. ELISEEV, IGOR I. MOKHOV**

*A.M. Obukhov Institute of Atmospheric Physics, RAS, Moscow, Russia*

8 **GEORG FEULNER, HENDRIK KIENERT, MAHÉ PERRETTE**

**THOMAS SCHNEIDER VON DEIMLING**

*Potsdam Institute for Climate Impact Research, Potsdam, Germany*

9

CHRIS E. FOREST

*Pennsylvania State University, College Park, Pennsylvania, USA*

10

PIERRE FRIEDLINGSTEIN

*University of Exeter, Exeter, UK*

11

FORTUNAT JOOS, RENATO SPAHNI, MARCO STEINACHER

*Physics Institute, University of Bern, Bern, Switzerland*

*Oeschger Centre for Climate Change Research, University of Bern, Bern, Switzerland*

12

MICHIO KAWAMIYA, KAORU TACHIIRI

*Research Institute for Global Change, JAMSTEC, Yokohama, Japan*

13

DAVID KICKLIGHTER

*The Ecosystems Center, MBL, Woods Hole, Massachusetts, USA*

14

ERWAN MONIER, ADAM SCHLOSSER, ANDREI SOKOLOV

*Massachusetts Institute of Technology, Cambridge, Massachusetts, USA*

15

KATSUMI MATSUMOTO, KATHY S. TOKOS

*University of Minnesota, Minneapolis, Minnesota, USA*

16

STEFFEN M. OLSEN

*Danish Meteorological Institute, Copenhagen, Denmark*

17

JENS O. P. PEDERSEN

*National Space Institute, Technical University of Denmark, Kgs. Lyngby, Denmark*

18

ANDY RIDGWELL

*School of Geographical Sciences, University of Bristol, Bristol, United Kingdom*

19

GARY SHAFFER

*Department of Geophysics, University of Concepcion, Concepcion, Chile*

*Niels Bohr Institute, University of Copenhagen, Copenhagen, Denmark*

20

MASAKAZU YOSHIMORI

*University of Tokyo, Tokyo, Japan*

21

NING ZENG, FANG ZHAO

*University of Maryland, College Park, Maryland, USA*

---

\**Corresponding author address:* Kirsten Zickfeld, Department of Geography, Simon Fraser University, 8888 University Drive, Burnaby, BC, V5A1S6.

E-mail: kzickfel@sfu.ca

## ABSTRACT

23 This paper summarizes the results of an intercomparison project with Earth System Models  
24 of Intermediate Complexity (EMICs) undertaken in support of the Intergovernmental Panel  
25 on Climate Change (IPCC) Fifth Assessment Report (AR5). The focus is on long-term  
26 climate projections designed to: (i) quantify the climate change commitment of different ra-  
27 diative forcing trajectories, and (ii) explore the extent to which climate change is reversible  
28 on human timescales. All commitment simulations follow the four Representative Concen-  
29 tration Pathways (RCPs) and their extensions to 2300. Most EMICs simulate substantial  
30 surface air temperature and thermosteric sea level rise commitment following stabilization  
31 of the atmospheric composition at year-2300 levels. The meridional overturning circulation  
32 (MOC) is weakened temporarily and recovers to near pre-industrial values in most models  
33 for RCPs 2.6–6.0. The MOC weakening is more persistent for RCP 8.5. Elimination of  
34 anthropogenic CO<sub>2</sub> emissions after 2300 results in slowly decreasing atmospheric CO<sub>2</sub> con-  
35 centrations. At year 3000 atmospheric CO<sub>2</sub> is still at more than half its year-2300 level in  
36 all EMICs for RCPs 4.5–8.5. Surface air temperature remains constant or decreases slightly  
37 and thermosteric sea level rise continues for centuries after elimination of CO<sub>2</sub> emissions in  
38 all EMICs. Restoration of atmospheric CO<sub>2</sub> from RCP to pre-industrial levels over 100–1000  
39 years requires large artificial removal of CO<sub>2</sub> from the atmosphere and does not result in the  
40 simultaneous return to pre-industrial climate conditions, as surface air temperature and sea  
41 level response exhibit a substantial time lag relative to atmospheric CO<sub>2</sub>.

# 1. Introduction

This paper summarizes the results of a model intercomparison project undertaken in support of the Fifth Assessment Report (AR5) of the Intergovernmental Panel on Climate Change (IPCC). Fifteen groups running Earth System Models of Intermediate Complexity (EMICs) participated in the intercomparison. Coordinated experiments include simulations of the climate of the past millennium and simulations of long-term future climate change, in addition to a set of idealized experiments. This paper will discuss the future climate projections, while the idealized and last-millennium simulations are the focus of a separate paper (Eby et al. 2013). The goals of the future climate simulations are to: (i) quantify the long-term climate change commitment in response to different radiative forcing trajectories, and (ii) explore the extent to which climate change is reversible if atmospheric CO<sub>2</sub> is left to evolve freely or is artificially restored to pre-industrial levels.

Climate change commitment refers to the climate changes that are to be expected in the future in response to past human activities. The concept of commitment is tied to the thermal inertia of the climate system (Hansen et al. 1985), which causes the effects of greenhouse gas emissions to be felt beyond the duration of those emissions. Climate change commitment is a useful metric for climate science and policy, as it quantifies the minimum climate change humanity faces, and represents a benchmark against which to measure the effect of future emissions. Most studies consider the “warming commitment”, but here we use the broader term “climate change commitment” to include other aspects of climate change such as sea level rise (Wigley 2005).

Different forms of climate change commitment have been discussed in the literature. The most prominent is the “constant composition” commitment, which refers to the climate changes that are to be expected after stabilization of the chemical composition of the atmosphere, and hence the radiative forcing, at a specified level (Wigley 2005; Meehl et al. 2005; Hare and Meinshausen 2006). This commitment was highlighted in the IPCC Fourth Assessment Report (AR4) and has been estimated at between 0.3°C and 0.9°C for the period

69 2090–2099 relative to 1980–1999 if the atmospheric composition is stabilized at year 2000  
70 levels (Meehl et al. 2007).

71 Another type of commitment, which has received greater attention more recently, is the  
72 “zero-emissions” commitment, which is the warming that is to be expected after complete  
73 elimination of emissions (Hare and Meinshausen 2006; Matthews and Caldeira 2008; Plattner  
74 et al. 2008; Eby et al. 2009; Lowe et al. 2009; Froelicher and Joos 2010; Solomon et al. 2010;  
75 Gillett et al. 2011; Zickfeld et al. 2012; Matthews and Zickfeld 2012). Most studies have  
76 explored the climate response to elimination of CO<sub>2</sub> emissions only. These studies have  
77 shown that instantaneous elimination of CO<sub>2</sub> emissions results in approximately constant  
78 global mean temperature for several centuries after emissions cease. When emissions of  
79 non-CO<sub>2</sub> greenhouse gases and aerosols also cease (Hare and Meinshausen 2006; Solomon  
80 et al. 2010; Froelicher and Joos 2010; Armour and Roe 2011; Matthews and Zickfeld 2012),  
81 the climate warms for about a decade and then gradually cools. The initial warming is  
82 due to the fast elimination of the negative radiative forcing associated with aerosols, which  
83 have a short atmospheric residence time. Greenhouse gases, on the other hand, have a  
84 longer atmospheric lifetime and their concentration and associated radiative forcing decline  
85 gradually after elimination of emissions. After about a century, the response is largely  
86 dominated by the long-lived CO<sub>2</sub> and the rate of cooling converges to that obtained under  
87 elimination of CO<sub>2</sub> emissions alone. Matthews and Weaver (2010) argue that the zero  
88 emission commitment is a more useful measure of climate change commitment, because  
89 it does not convolute the physical response of the climate system to past emissions with the  
90 response to future emissions that are needed to maintain the atmospheric CO<sub>2</sub> concentration  
91 at stable levels, as for the constant composition commitment.

92 Another form of climate change commitment is the “constant emissions” commitment,  
93 which refers to the climate changes to be expected in response to constant anthropogenic  
94 emissions (Wigley 2005; Hare and Meinshausen 2006; Meinshausen et al. 2011b). This type  
95 of commitment is less prominently discussed in the literature. A study with a simple climate



96 model (MAGICC) calibrated to Atmosphere-Ocean General Circulation Models (AOGCMs)  
97 (Meinshausen et al. 2011a) estimates the constant emissions commitment at 1–2.5°C by 2100  
98 (relative to 2000) assuming constant year-2010 emissions (Collins et al. 2013).

99 The second set of experiments which is part of this model intercomparison is aimed at  
100 exploring the extent to which the climate system can revert to “safe” levels, should climate  
101 change impacts turn out to be “dangerous”. Insight gained from zero emission commit-  
102 ment simulations suggests that because of the long residence time of CO<sub>2</sub> in the atmosphere  
103 (Archer and Brovkin 2008; Eby et al. 2009) and the large thermal reservoir of the ocean,  
104 complete elimination of emissions can at best lead to stable or slowly decreasing tempera-  
105 tures. If permafrost carbon feedbacks are considered, elimination of emissions could lead to a  
106 continuing increase in temperature (MacDougall et al. 2012). Therefore, restoring tempera-  
107 ture to lower levels in a time frame meaningful to human societies can only be accomplished  
108 with “negative emissions” i.e. net removal of carbon dioxide from the atmosphere. Such  
109 negative emissions can be achieved, for instance, by biomass energy in combination with  
110 capture and geological storage of the emitted CO<sub>2</sub> (BECS) (Azar et al. 2006), or by CO<sub>2</sub>  
111 “scrubbers” which remove the CO<sub>2</sub> directly from the atmosphere (Keith et al. 2006).

112 Few studies to date have explored the response of the climate system to scenarios with  
113 negative emissions or “overshoot” scenarios (Yoshida et al. 2005; Tsutsui et al. 2007; Nus-  
114 baumer and Matsumoto 2008; Zickfeld et al. 2012). Most of these studies use idealized sce-  
115 narios, such as atmospheric CO<sub>2</sub> increasing gradually to two or four times the pre-industrial  
116 level and then decreasing at a similar rate (Held et al. 2010; Boucher et al. 2012). These stud-  
117 ies suggest that because of the long timescales of components of the climate system, global  
118 mean temperature, precipitation, ocean heat content and other quantities lag the forcing and  
119 revert to the target level only slowly. The residual change (i.e. the difference between the  
120 target and the actual level) increases with the level of peak forcing (Held et al. 2010; Boucher  
121 et al. 2012). The idealized scenarios used in these papers, which entail large and abrupt de-  
122 creases in atmospheric CO<sub>2</sub>, imply levels of negative emissions that are likely beyond known

123 technological capabilities (McGlashan et al. 2012). The set of scenarios used for the Coupled  
124 Model Intercomparison Project Phase 5 (CMIP5) (Taylor et al. 2008) includes one scenario  
125 with moderate negative emissions which is based on plausible technological and economic  
126 assumptions (Representative Concentration Pathway (RCP) 2.6; Moss et al. (2010)).

127 In this paper, we analyze multi-century constant composition, zero emissions and con-  
128 stant emissions commitment simulations with EMICs under a range of radiative forcing  
129 scenarios. In addition, we investigate the EMICs’ response to a set of reversibility scenar-  
130 ios, whereby atmospheric CO<sub>2</sub> is artificially restored to pre-industrial levels, or is left to  
131 evolve freely after a millennium of constant radiative forcing. Finally, we explore the cu-  
132 mulative CO<sub>2</sub> emissions that are compatible with climate stabilization targets using inverse  
133 simulations with two EMICs.

134 The paper is organized as follows. In Section 2 we briefly introduce the EMICs that par-  
135 ticipated in the model intercomparison and describe the experimental setup. In Section 3 the  
136 results of the model simulations are presented and discussed with reference to the literature.  
137 The section starts with a discussion of the ability of EMICs to simulate the climate of the  
138 20<sup>th</sup> century, continues with a description of the results of the climate change commitment  
139 and reversibility simulations and ends with a discussion of cumulative emissions compatible  
140 with long-term climate targets. Section 4 presents a summary and conclusions.

## 141 **2. Methods**

### 142 *a. Participating Models*

143 This study includes results from twelve EMICs, eight of which are coupled climate-carbon  
144 cycle models. The models are the University of Bern three-dimensional Earth system model  
145 (Bern3D-LPJ) (Ritz et al. 2011; Stocker et al. 2011), versions 2.4 and 3 $\alpha$  of the Potsdam  
146 Institute climate and biosphere model (CLIMBER-2.4, CLIMBER-3 $\alpha$ ) (Petoukhov et al.  
147 2000; Montoya et al. 2005), version 1.0 of the Danish Centre for Earth System Science

148 (DCESS) Earth System model (Shaffer et al. 2008), release 2-2-7 of the GENIE Earth system  
149 model adapted with an implementation of land use change (Holden et al. 2013), the A.M  
150 Obukhov Institute of Atmospheric Physics, Russian Academy of Sciences climate model  
151 (IAP RAS CM) (Eliseev and Mokhov 2011), version 2.2 of the Massachusetts Institute of  
152 Technology’s Integrated Global System Model (IGSM2.2) (Sokolov et al. 2005), version 1.2 of  
153 the LOVECLIM Earth System Model (LOVECLIM 1.2) (Goosse et al. 2010), version 1.0 of  
154 the MESMO Earth System Model (MESMO 1.0) (Matsumoto et al. 2008), the MIROC-lite-  
155 LCM Earth System model (Tachiiri et al. 2010), version 2.0 of the University of Maryland  
156 Coupled Atmosphere-Biosphere-Ocean model (UMD 2.0) (Zeng et al. 2004), and version  
157 2.9 of the University of Victoria Earth System Climate Model (UVic 2.9) (Weaver et al.  
158 2001; Eby et al. 2009). The characteristics of each model are briefly described in the EMIC  
159 intercomparison companion paper (Eby et al. 2013).

160 A common trait of these models is that they are simplified, i.e. include processes in a  
161 more parameterized form and have generally lower resolution compared to atmosphere-ocean  
162 general circulation models (AOGCMs) and complex Earth System Models (ESMs). The  
163 group of EMICs, however, is very heterogeneous, ranging from zonally averaged (Petoukhov  
164 et al. 2000) or mixed layer ocean models (Sokolov et al. 2005) coupled to statistical-dynamical  
165 models of the atmosphere to low-resolution three-dimensional ocean general circulation mod-  
166 els coupled to simplified dynamical models of the atmosphere (Goosse et al. 2010). Eight  
167 out of twelve models include an interactive carbon cycle (Bern3D-LPJ, DCESS, GENIE,  
168 IGSM2.2, MESMO, MIROC-lite-LCM, UMD, UVic 2.9). Of these, several models calcu-  
169 late land-use emissions internally (Bern3D-LPJ, GENIE, IGSM,UVic 2.9) and/or represent  
170 seafloor sediment processes, including deep water carbonate sedimentation (Bern3D-LPJ,  
171 DCESS, GENIE, UVic 2.9).

172 *b. Experimental Design*

173 Most models were spun up with year-850 forcing. The models were then integrated from  
174 850 to 2005 using known natural (orbital, volcanic, solar) and anthropogenic (greenhouse  
175 gas, aerosol, land-cover change) forcing, following the PMIP3/CMIP5 protocol. Details on  
176 the implementation of these forcings in individual EMICs is provided in the Appendix of the  
177 EMIC intercomparison companion paper (Eby et al. 2013). Note that in this paper we only  
178 consider the 1850–2005 portion of the last millennium simulation (henceforth referred to as  
179 the “historical” or HIST simulation). The full simulation is discussed in detail in Eby et al.  
180 (2013). The MIROC-lite-LCM model was spun up with year-1850 forcing and integrated  
181 from 1850 to 2005.

182 Starting from the end point of the historical simulation, models were integrated with CO<sub>2</sub>  
183 concentration and non-CO<sub>2</sub> greenhouse gas forcing specified according to four Representa-  
184 tive Concentration Pathways (RCPs) (from 2006 to 2100) and their extensions (to 2300)  
185 (Meinshausen et al. 2011b). Aerosol forcing (direct effect) and land-cover change followed  
186 RCP specifications until 2100 and were held constant thereafter. Natural forcings were spec-  
187 ified as follows: orbital forcing was held fixed at year-2005 levels, solar irradiance was set to  
188 repeat the last solar cycle (1996–2008) and volcanic forcing was set to zero.

189 The atmospheric CO<sub>2</sub> concentration of the four RCPs (RCP2.6, RCP4.5, RCP6.0, RCP8.5)  
190 and their extensions is shown in Figure 1.

191 From year 2301 to 3000 a set of climate change commitment simulations was performed  
192 for all four RCPs. In the constant composition commitment (CCO) simulations, atmospheric  
193 CO<sub>2</sub> concentration and the forcing from non-CO<sub>2</sub> greenhouse gases were held constant at  
194 year-2300 levels. Other forcings were held fixed at the level specified for the RCP simulations.  
195 A slightly different simulation protocol was followed for the MIROC-lite-LCM, with constant  
196 solar forcing after 2300 (no solar cycle). EMICs with a carbon cycle diagnosed the CO<sub>2</sub>  
197 emissions compatible with the specified CO<sub>2</sub> concentration trajectories.

198 The commitment runs described in the following were performed with climate-carbon

199 cycle models only. In a second set of simulations, which we designate as the “pre-industrial  
200 CO<sub>2</sub> emission commitment” experiments (PIEM-CO<sub>2</sub>), the “anthropogenic CO<sub>2</sub> perturba-  
201 tion” - defined as the difference in implied CO<sub>2</sub> emissions between the last decade of the RCP  
202 simulations (2290–2300) and the decade 1840–1850 of the historical simulation - was set to  
203 zero starting in 2300, while the radiative forcing from non-CO<sub>2</sub> greenhouse gases was held  
204 fixed at year-2300 levels. Other forcings were held fixed at the level specified for the RCP  
205 simulations. For the GENIE model, CO<sub>2</sub> emissions were set to zero after 2300. It should  
206 be noted that in most models, setting the anthropogenic perturbation to zero did not result  
207 in zero emissions exactly. The reason is that the 1840–1850 land-atmosphere and ocean-  
208 atmosphere CO<sub>2</sub> fluxes in response to forcing are not exactly consistent with the specified  
209 atmospheric CO<sub>2</sub>. Diagnosed emissions are negative in all models (except UMD), implying  
210 a flux of CO<sub>2</sub> from the land and ocean into the atmosphere. Processes responsible for the  
211 excess emissions could be the warming recovery after volcanic eruption, or land use change.

212 In the pre-industrial emission simulations (PIEM), CO<sub>2</sub> emissions after 2300 were spec-  
213 ified as in the PIEM-CO<sub>2</sub> simulation, but the radiative forcing from non-CO<sub>2</sub> greenhouse  
214 gases was set to 1840–1850 average levels. Other forcings were held fixed at the level specified  
215 for the RCP simulations.

216 In the constant emissions commitment (CEM) simulations, implied CO<sub>2</sub> emissions over  
217 the last decade of the RCP integrations (years 2290-2300) were diagnosed, and CO<sub>2</sub> emissions  
218 held fixed at this value from 2300 onwards. Radiative forcing from non-CO<sub>2</sub> greenhouse gases  
219 was held constant at year-2300 levels and other forcings were held fixed at the level specified  
220 for the RCP simulations.

221 In addition to the commitment simulations, a set of reversibility runs (RE) was also  
222 performed by several EMIC groups. These simulations start from the year-3000 model  
223 configuration of the constant composition commitment (CCO) experiments and extend to  
224 the year 4000. In the first experiment (REa), atmospheric CO<sub>2</sub> decreases linearly to the  
225 pre-industrial level over 100 years, while non-CO<sub>2</sub> forcings are held fixed at year-3000 lev-

226 els. Forcing specifications are similar in the second experiment (REb), except that CO<sub>2</sub>  
227 is prescribed to decrease to pre-industrial levels over a period of 1000 years. In the third  
228 experiment (REc), atmospheric CO<sub>2</sub> is allowed to evolve freely (zero CO<sub>2</sub> emissions) and  
229 non-CO<sub>2</sub> forcings are again held fixed at year-3000 levels. REc experiments with freely  
230 evolving atmospheric CO<sub>2</sub> were performed by EMICs with an interactive carbon cycle only.

231 Finally, a set of simulations was carried out whereby a temperature stabilization trajec-  
232 tory was specified, and the cumulative emissions consistent with that temperature trajectory  
233 were calculated, following the inverse modelling approach described in Zickfeld et al. (2009).  
234 Four “temperature tracking” (TTR) simulations were performed, with global mean surface  
235 air temperatures stabilizing at 1.5°C, 2°C, 3°C and 4°C warming relative to pre-industrial.  
236 The simulations started from the end of the historical simulation and were integrated to  
237 year 2500. Natural forcings were specified as in the RCP simulations. Land-use change was  
238 held constant at the year-2005 pattern, whereas non-CO<sub>2</sub> greenhouse gas and aerosol forcing  
239 linearly decreased from year-2005 values to zero by 2300.

240 All model simulations are summarized in Table 1.

## 241 **3. Results and Discussion**

### 242 *a. Historical simulation*

243 The performance of EMICs over the historical period is discussed in detail in Eby et al.  
244 (2013). Here, we briefly summarize the main findings to allow the reader to put the EMICs’  
245 future projections and their uncertainty ranges into perspective.

246 Over the 20<sup>th</sup> century EMICs simulate a model ensemble mean warming of 0.78°C (range:  
247 0.4–1.2°C), compared to the observed warming of 0.73°C (Morice et al. 2013) over the same  
248 period (Table 2). Five models stay mostly within the observational uncertainty envelope for  
249 this period, five tend to overestimate the observed warming and two tend to underestimate it  
250 (Eby et al. (2013), Figure 1b). The spread in models is due to different climate sensitivities

251 and differences in the specification of radiative forcing, particularly from land-use change  
252 and tropospheric aerosols (Eby et al. 2013).

253 EMICs simulate a model-mean rate of ocean thermal expansion for 1971–2010 of  $1.1 \text{ mm yr}^{-1}$   
254 compared to the observations-based estimate of  $0.8 \text{ mm yr}^{-1}$  (Rhein et al. 2013). Eight  
255 EMICs are within the uncertainty range of observed values, and four overestimate thermal  
256 expansion. Ocean thermal expansion is determined by both the models’ heat uptake efficacy  
257 and climate sensitivity, which differ largely between models (Eby et al. 2013, Table 2).

258 The atmospheric  $\text{CO}_2$  concentration was specified in the historical simulation and EMICs  
259 with an interactive carbon cycle were used to diagnose the  $\text{CO}_2$  emissions compatible with  
260 the specified  $\text{CO}_2$  concentrations. The average EMIC carbon cycle response for the 1990s is  
261 within the uncertainty range of observed values (Denman et al. 2007), except for diagnosed  
262 emissions, which are slightly underestimated (Table 2). Ocean fluxes simulated by all but  
263 one EMICs are within the uncertainty range of observed values. Although the EMIC average  
264 land fluxes fall within the large range of uncertainty, several models underestimate both the  
265 land use change flux and the residual land flux (i.e. the total land-atmosphere flux minus  
266 the land use change flux).

267 The EMICs’ cumulative carbon fluxes from 1800 to 1994 are compared to estimates from  
268 Sabine et al. (2004). Again, all models estimate total ocean uptake within the uncertainty  
269 range of observed values (Table 2). Land uptake differs largely between models, with only  
270 half of the models’ simulated fluxes falling within the estimated uncertainty range. EMICs  
271 whose land flux agrees well with observation also simulate 1800–1994 cumulative emissions  
272 within the observed range.

273 Overall, the 20<sup>th</sup> century climate and carbon cycle response simulated by EMICs agrees  
274 reasonably well with observations, which supports the use of EMICs to project long-term  
275 climate change and to complement more complex AOGCMs and Earth System models.

276 *b. Constant composition commitment*

277 Figure 2 shows the time evolution of physical climate variables for the constant composi-  
278 tion commitment simulations. At the multi-century time scale considered in this study, the  
279 warming depends strongly on the forcing scenario, being highest in RCP8.5 and lowest in the  
280 low emission RCP2.6 scenario. Following the radiative forcing, the model ensemble mean  
281 temperature under the RCP2.6 scenario peaks at 2070 and declines until reaching a mini-  
282 mum in 2300, after which it slowly increases again. Global mean temperature under RCP2.6  
283 peaks at 1.0°C relative to 1986–2005 in the ensemble mean (model range: 0.6–1.5°C) and  
284 decreases to 0.6°C (0.3–1.1°C) at 2300. Assuming an observed warming of 0.7°C between  
285 1850 and 2005, the ensemble mean peak and year-2300 warming are 1.7°C and 1.3°C above  
286 pre-industrial, respectively. In a few models, however, peak warming exceeds 2.0°C relative  
287 to preindustrial (Fig. 3).

288 Under the other RCP scenarios (RCP4.5, RCP6.0, RCP8.5) the global temperature in-  
289 creases rapidly until the time of stabilization of the forcing, and more slowly thereafter. By  
290 2300, global warming approaches 2.2°C under RCP4.5, 3.3°C under RCP6.0, and 7.0°C un-  
291 der RCP8.5 in the ensemble mean (relative to 1986–2005). The ensemble means and model  
292 ranges are generally consistent with those simulated by AOGCMs and Earth System models  
293 contributing to the CMIP5 (Table 3).

294 Most EMICs simulate a considerable warming commitment following stabilization of ra-  
295 diative forcing at year-2300 levels. The continuing albeit slower warming after stabilization  
296 is a well known feature of climate models and is associated with the large thermal inertia  
297 of the ocean (Hansen et al. 1985). IPCC AR4 models estimated the additional warming  
298 after stabilization of the atmospheric composition at year-2000 levels at 0.6°C for the pe-  
299 riod 2090–2099 relative to 1980–1999 (Meehl et al. 2007), or 0.3°C relative to 2000 (Collins  
300 et al. 2013). AOGCM simulations in support of IPCC AR5 do not include a year-2000 con-  
301 stant composition commitment simulation. It is possible, however, to estimate the warming  
302 commitment for the RCP4.5 scenario and its extension: it amounts to 0.8°C between 2100



303 (the time of stabilization of the radiative forcing) and 2300 (Collins et al. 2013, Table 12.2).  
304 In this study the model mean warming between 2100 and 2300 is 0.3–0.4°C for RCPs 4.5,  
305 6.0 and 8.5, somewhat lower than the CMIP5 estimate. The additional warming between  
306 2300 and 3000 is 0.3°C, 0.4°C and 0.7°C in the ensemble mean for RCPs 4.5, 6.0 and 8.5,  
307 respectively, indicating a slight increase with radiative forcing. Another measure of constant  
308 composition commitment is the fraction of realized warming (Solomon et al. 2009), which is  
309 here estimated as the ratio of warming at a given time to the warming averaged over the last  
310 two decades of the simulation (2981–3000) (Fig. 2). At the time of stabilization of radiative  
311 forcing, the fraction of realized warming is ~70–90% in the ensemble mean for RCPs 4.5,  
312 6.0 and 8.5.

313 Sea level rise due to thermal expansion (“thermosteric” sea level rise) continues for cen-  
314 turies after stabilization of radiative forcing in all scenarios due to the long response time  
315 scale of the deep ocean. Despite the peaking and declining radiative forcing under RCP2.6,  
316 the rate of thermosteric sea level rise is positive throughout the duration of the simulation in  
317 all models (Fig 2). Thermal expansion simulated by EMICs for the four RCPs and selected  
318 time periods is given in Table 3. The model mean thermal expansion by 2100 agrees very  
319 well with that simulated by CMIP5 models.

320 The thermosteric sea level rise commitment after stabilization of radiative forcing is  
321 substantial under RCPs 4.5, 6.0 and 8.5 and at 3000 amounts to 1.5–3 times the thermosteric  
322 sea level rise at the time of forcing stabilization. Note that none of the EMICs include  
323 sea level rise due to melting of land-based glaciers and ice sheets. Consideration of these  
324 contributions would lead to substantially higher sea level rise estimates, but the exact value  
325 is highly uncertain due to incomplete understanding of glacier and ice sheet dynamics.

326 The Atlantic meridional overturning circulation (MOC) weakens under all scenarios  
327 (Fig. 2). Under RCPs 2.6, 4.5 and 6.0 the weakening is temporary, and the circulation  
328 recovers to within 80% of the pre-industrial strength at the end of the simulation in most  
329 models. Under RCP8.5 the weakening is more persistent, and the model ensemble mean

330 MOC recovers to 60% of the pre-industrial strength at 3000. Under this scenario the MOC  
331 response varies considerably among models: while in some models the circulation recovers  
332 to near pre-industrial values, it is close to a complete collapse in the Bern3D-LPJ EMIC.

333 Comparison of constant composition commitment estimates with those from an earlier  
334 EMIC intercomparison (Plattner et al. 2008) is hampered by the use of different scenarios  
335 (SRES as opposed to RCP) and set of models used. However, given the similarity of the  
336 SRES B1 stabilization scenario and RCP 4.5 (in both scenarios atmospheric CO<sub>2</sub> stabilizes at  
337 550 ppmv) we attempted a comparison of the warming and thermal expansion commitment  
338 for these two scenarios. The additional warming between years 2100 and 3000 is larger  
339 in Plattner et al. (2008) than in this study (0.6–1.6°C for SRES B1 versus 0.1–1.2°C for  
340 RCP 4.5), but with a similar inter-model range ( $\sim 1.0^\circ\text{C}$ ). Thermal expansion commitment  
341 is similar in the two studies, with the range simulated in this study encompassing the range  
342 of Plattner et al. (2008) (0.3–1.1 m for SRES B1 versus 0.2–1.4 m for RCP 4.5). Differences  
343 in warming and thermal expansion commitment may be due to the different set of models  
344 used in the two intercomparisons, but also differences in non-CO<sub>2</sub> forcing between scenarios.

345 EMICs with an interactive carbon cycle were used to diagnose the CO<sub>2</sub> emissions compat-  
346 ible with the CO<sub>2</sub> concentration pathways specified under the constant composition commit-  
347 ment simulations. Diagnosed CO<sub>2</sub> emissions are estimated by closing the global-mean carbon  
348 budget of the atmosphere and are determined by the atmosphere-land and atmosphere-ocean  
349 CO<sub>2</sub> fluxes. Figure 4 shows CO<sub>2</sub> emissions and changes in carbon inventories since 1850 sim-  
350 ulated by eight EMICs for scenario RCP2.6. CO<sub>2</sub> emissions peak around 2020, and decline  
351 steeply thereafter. Since the rate of atmospheric CO<sub>2</sub> decrease exceeds the rate of CO<sub>2</sub>  
352 uptake by carbon sinks, diagnosed emissions become negative in all models. Minimum emis-  
353 sions range from  $-1.5 \text{ PgCyr}^{-1}$  to  $-0.5 \text{ PgCyr}^{-1}$ . After stabilization of atmospheric CO<sub>2</sub>,  
354 emissions settle at a slightly positive value (equal to the rate of CO<sub>2</sub> uptake by carbon  
355 sinks). Cumulative CO<sub>2</sub> emissions since 1850 vary substantially among models despite iden-  
356 tical prescribed atmospheric CO<sub>2</sub> and range from 300 PgC to 830 PgC at 2300 and from

357 380 PgC to 1040 PgC at year 3000. The airborne fraction of cumulative emissions decreases  
358 from 45–70% at the time of peak atmospheric CO<sub>2</sub> (year 2050) to 15–42% at the end of the  
359 simulation.

360 Accumulated land carbon uptake is negative at the year 2000 in all models that simulate  
361 land use change (LUC) emissions interactively on the basis of land cover changes (all EMICs  
362 except MESMO, UMD). The reason is that CO<sub>2</sub> emissions due to land-use exceed net CO<sub>2</sub>  
363 uptake by vegetation during most of the historical period (Eby et al. 2013). Between 2000  
364 and the year of peak atmospheric CO<sub>2</sub>, the terrestrial biosphere acts as a sink of CO<sub>2</sub> in  
365 most models (except in Bern3D-LPJ and UVic). Between the CO<sub>2</sub> peak and the time of CO<sub>2</sub>  
366 stabilization, the terrestrial biosphere becomes a source of CO<sub>2</sub> in all models. The range in  
367 land carbon uptake under the RCP2.6 scenario is spanned by the UMD model at the upper  
368 end, which has a small land uptake sensitivity to CO<sub>2</sub> ( $\beta_L$ ) but also a small sensitivity to  
369 temperature ( $\gamma_L$ ) (Eby et al. 2013) and does not simulate LUC emissions, and the Bern3D-  
370 LPJ and UVic models at the lower end (both models have large land uptake sensitivities to  
371 CO<sub>2</sub> but also medium to large sensitivities to temperature and do simulate LUC emissions).  
372 The fraction of cumulative emissions taken up by the land (land uptake fraction) decreases  
373 between 2100 and 2300 and remains approximately constant thereafter.

374 The ocean takes up carbon from the atmosphere throughout the duration of the RCP 2.6  
375 constant composition simulation in all models. Ocean carbon uptake slows after the peak in  
376 atmospheric CO<sub>2</sub> and accelerates again after CO<sub>2</sub> is stabilized. Accumulated ocean carbon  
377 uptake is larger than accumulated land carbon uptake at all times in all models. The range  
378 in ocean carbon uptake is spanned by the UMD model at the upper end (highest ocean  
379 carbon uptake sensitivity to CO<sub>2</sub>,  $\gamma_O$ ; Eby et al. (2013)) and the UVic model (low carbon  
380 uptake sensitivity to CO<sub>2</sub>). The ocean uptake fraction increases continuously between the  
381 time of peak CO<sub>2</sub> and 2300, and remains approximately constant thereafter.

382 Figure 5 displays changes in carbon inventories in the year 3000 for constant composition  
383 commitment simulations under all four RCPs. Diagnosed cumulative CO<sub>2</sub> emissions increase

384 approximately linearly with atmospheric CO<sub>2</sub> for RCPs 2.6–6.0, but the increase becomes less  
385 than linear at higher radiative forcing in most models. The spread in cumulative emissions  
386 diagnosed by models also increases with higher atmospheric CO<sub>2</sub>, with a range as large as  
387 4,500–11,500 PgC for RCP8.5. Cumulative emissions at the upper end of this range are close  
388 to estimates of the carbon bound in the total fossil fuel resource base (9,500–15,600 PgC;  
389 GEA (2012)).

390 The airborne fraction increases with increasing atmospheric CO<sub>2</sub>, from a model ensemble  
391 mean of 0.27 for RCP2.6 to 0.57 for RCP8.5. The increase in airborne fraction with CO<sub>2</sub> is  
392 mostly a result of the decreasing ocean uptake fraction.

393 Ocean carbon uptake is largely driven by atmospheric CO<sub>2</sub>, with the lowest cumulative  
394 uptake occurring in RCP2.6 and the largest in RCP8.5. The ocean uptake fraction decreases  
395 significantly with higher CO<sub>2</sub> in all models, from an ensemble mean value of 0.89 in RCP2.6  
396 to 0.44 in RCP8.5. The decrease in ocean uptake fraction is due to nonlinear ocean car-  
397 bonate chemistry and stronger climate-carbon cycle feedbacks at higher atmospheric CO<sub>2</sub>  
398 (Friedlingstein et al. 2006; Plattner et al. 2008).

399 The results for land carbon uptake are more complex, as they vary significantly across  
400 models and scenarios. In RCPs 4.5 and 6.0, the terrestrial biosphere takes up carbon be-  
401 tween 2000 and the year of CO<sub>2</sub> stabilization in all models (not shown). In RCP8.5, the  
402 terrestrial biosphere initially takes up CO<sub>2</sub>, but becomes a CO<sub>2</sub> source after about a century  
403 in most models. The Bern3D-LPJ exhibits negligible land uptake even in the first hundred  
404 years of the RCP8.5 simulation. After CO<sub>2</sub> stabilization, the land response ranges from  
405 strong emissions (Bern3D-LPJ) to weak uptake (UVic) under all RCPs (not shown). RCP  
406 differences in land carbon uptake during the 21<sup>st</sup> century result from different strengths of  
407 carbon cycle feedbacks, but also differences in land cover change. For instance, RCPs 4.5  
408 and 6.0 include reforestation, while RCPs 2.6 and 8.5 assume substantial deforestation.

409 The behavior of land carbon uptake at 3000 as a function of atmospheric CO<sub>2</sub> varies  
410 strongly across models: while some EMICs simulate an increase in land uptake with in-

411 creasing CO<sub>2</sub> (e.g. DCESS), others simulate a strong decrease (Bern3D-LPJ) (Fig. 5c).  
412 Bern3D-LPJ has the highest sensitivity of land carbon uptake to temperature (Eby et al.  
413 2013), as it includes a representation of carbon release from permafrost soils and peatlands.  
414 The land uptake fraction increases from RCP2.6 to RCP4.5 in most models, and remains  
415 approximately constant or decreases from RCP4.5 to RCP8.5 (the ensemble mean land up-  
416 take fraction remains approximately constant across RCPs). The low land uptake fraction  
417 under RCP2.6 in some models may be due to relatively large LUC emissions (Arora et al.  
418 2011).

419 Our results differ from those of a previous EMIC intercomparison (Plattner et al. 2008),  
420 which found that the fractional distribution of excess carbon among the atmosphere, ocean  
421 and terrestrial biosphere remained approximately constant across scenarios. That study,  
422 however, considered a much narrower range in atmospheric CO<sub>2</sub> changes ( $\sim 700$ – $1000$  PgC).

### 423 *c. Pre-industrial CO<sub>2</sub> emission commitment*

424 Pre-industrial CO<sub>2</sub> emission commitment (PIEM-CO<sub>2</sub>) is investigated by setting the  
425 anthropogenic CO<sub>2</sub> emission perturbation to zero after 2300 and letting the atmospheric  
426 CO<sub>2</sub> concentration evolve freely. Non-CO<sub>2</sub> radiative forcing is held constant at year-2300  
427 levels. These simulations were performed by EMICs with an interactive carbon cycle only.  
428 As discussed in section 2b, setting the anthropogenic perturbation to zero does not result in  
429 zero emissions exactly: decadal-mean CO<sub>2</sub> emissions after 2300 range from  $-0.5$  PgCyr<sup>-1</sup> to  
430  $0.5$  PgCyr<sup>-1</sup> for all RCPs (Fig. 6). CO<sub>2</sub> emissions are  $\leq 0$  in all models, except for the UMD  
431 model. The long-term effect of these annual emissions is evident in Fig. 7 for the RCP2.6  
432 PIEM-CO<sub>2</sub> commitment simulation, with cumulative emissions declining between 2300 and  
433 3000 (with exception of the UMD model, for which cumulative emissions increase). Note  
434 that despite the slightly different model setup, the PIEM-CO<sub>2</sub> commitment simulations are  
435 comparable to the zero-CO<sub>2</sub>-emission commitment simulations discussed in the literature.

436 As CO<sub>2</sub> emissions nearly cease, atmospheric CO<sub>2</sub> declines as the ocean and land continue

437 to absorb carbon from the atmosphere (Fig. 6). The efficacy of carbon uptake differs between  
438 models, and so does the rate of decline of atmospheric CO<sub>2</sub>. By the year 3000, atmospheric  
439 CO<sub>2</sub> is still far away from a new equilibrium due to the long timescales of CO<sub>2</sub> removal from  
440 the atmosphere (Eby et al. 2009). By 3000, the ensemble mean atmospheric CO<sub>2</sub> is 330 ppmv  
441 in RCP2.6, 440 ppmv in RCP4.5, 590 ppmv in RCP6.0 and 1560 ppmv in RCP8.5. Note  
442 that the upper boundary of the atmospheric CO<sub>2</sub> range spanned by models increases after  
443 2300. The upper limit is set by the UMD model, which has slightly positive CO<sub>2</sub> emissions.  
444 Atmospheric CO<sub>2</sub> at 3000 in RCPs 4.5–8.5 is still at a high fraction ( $\geq 0.5$ ) of the peak  
445 atmospheric CO<sub>2</sub> in all models (Fig. 8). These results are consistent with previous studies  
446 (Montenegro et al. 2007; Archer and Brovkin 2008; Plattner et al. 2008; Eby et al. 2009;  
447 Solomon et al. 2009; Archer et al. 2009), which showed that a significant fraction of CO<sub>2</sub>  
448 remains airborne after several hundred years, and that this fraction increases with higher  
449 CO<sub>2</sub> concentrations (or emissions).

450 Despite decreasing radiative forcing after 2300 in most models, global mean temperature  
451 decreases only slightly in RCPs 4.5–6.0 between 2300 and 3000 and remains approximately  
452 constant in RCP8.5 (Table 4). This near constancy of global mean temperature after elimina-  
453 tion of anthropogenic CO<sub>2</sub> emissions is known from earlier studies with EMICs and complex  
454 Earth System models (Matthews and Caldeira 2008; Plattner et al. 2008; Eby et al. 2009;  
455 Solomon et al. 2009; Lowe et al. 2009; Froelicher and Joos 2010; Gillett et al. 2011; Zickfeld  
456 et al. 2012) and results from the cancellation of two opposing effects: the delayed warming  
457 due to ocean thermal inertia and the decrease in radiative forcing associated with declin-  
458 ing atmospheric CO<sub>2</sub> levels in conjunction with the logarithmic dependence of forcing on  
459 atmospheric CO<sub>2</sub> (Eby et al. 2009; Solomon et al. 2010). At 3000, the fraction of warming  
460 that persists relative to that in the year 2300 (the year the anthropogenic perturbation is  
461 set to zero, which approximately corresponds to the year of peak warming) is 0.85, 0.89 and  
462 0.99 in the ensemble mean for RCPs 4.5, 6.0 and 8.5 respectively (Fig. 8). These values  
463 are consistent with those from Eby et al. (2009), who found that 80–100% of the warming

464 anomaly persists 700 years after emissions were eliminated, with the fraction increasing with  
465 the amount of cumulative emissions.

466 In contrast to global mean temperature, sea level rise due to thermal expansion continues  
467 after elimination of anthropogenic CO<sub>2</sub> emissions in RCPs 4.5–8.5. The sea level rise between  
468 2300 and 3000 is substantial in these scenarios (Table 4) and comparable to the sea level rise  
469 between 1850 and 2300. While sea level rise in some EMICs levels off toward the end of the  
470 simulation, it continues to rise in others. This is consistent with the results of a previous  
471 EMIC intercomparison (Plattner et al. 2008). In zero-emission commitment simulations with  
472 a complex Earth System Model, Gillett et al. (2011) found thermosteric sea level to still rise  
473 900 years after cessation of emissions. Given that surface air temperature remains elevated  
474 for centuries to millennia and intermediate-depth temperature in the high latitude Southern  
475 Ocean continues to warm, potentially leading to a collapse of the West Antarctic ice sheet  
476 (Gillett et al. 2011), thermal expansion on these timescales is likely to be compounded by  
477 large sea level contributions from disintegrating ice sheets.

478 Both global mean warming and sea level rise behave differently in RCP2.6 than in the  
479 higher scenarios (Fig. 7). Due to the strong decline in atmospheric CO<sub>2</sub> and, accordingly,  
480 radiative forcing already before 2300, the warming and sea level rise commitment after 2300  
481 are lower in this scenario. Global mean temperature continues to decrease between 2300 and  
482 3000 and sea level stabilizes or even starts to slightly drop in some models (except for the  
483 UMD model, for which atmospheric CO<sub>2</sub> increases after 2300).

484 An interesting question in view of the comparability of results from different studies is  
485 whether the pre-industrial (or zero) CO<sub>2</sub> emission commitment is dependent on the time  
486 CO<sub>2</sub> emissions cease. We address this question by comparing the temperature and thermal  
487 expansion commitment in PIEM-CO<sub>2</sub> simulations with those in the reversibility simulations  
488 (REc) with constant year-2300 radiative forcing to the year 3000 and zero CO<sub>2</sub> emissions  
489 thereafter. If CO<sub>2</sub> emissions cease earlier (e.g. in 2300 as opposed to 3000) the system is  
490 further away from equilibrium with the stabilized radiative forcing, the fraction of realized

491 warming is smaller (Fig. 2b), and one would expect a larger temperature and thermal ex-  
492 pansion commitment. One complicating factor in our comparison is that the PIEM-CO<sub>2</sub>  
493 simulations entail slightly negative (as opposed to zero) emissions in most models, leading  
494 to a more rapid decline in atmospheric CO<sub>2</sub> and hence radiative forcing after cessation of  
495 emissions. The model average decrease in surface air temperature after emissions cease is  
496 lower in the REc than in the PIEM-CO<sub>2</sub> simulations (-0.2°C versus -0.5°C for RCPs 4.5 and  
497 6.0), which we attribute to the slower decline in radiative forcing in the REc simulations. On  
498 the other hand, the thermal expansion commitment is larger in the PIEM-CO<sub>2</sub> simulations  
499 (0.3 m versus 0.1 m in the REc simulation for RCP 6.0), consistent with the smaller fraction  
500 of realized warming at the time emissions cease. These results indicate that the temperature  
501 commitment is determined largely by the radiative forcing after emissions cease, whereas  
502 the thermal expansion commitment is determined by the radiative forcing before emissions  
503 cease, consistent with the longer response timescale of the deep ocean.

504 *d. Pre-industrial emission commitment*

505 The pre-industrial emission commitment simulations (PIEM) are similar to the PIEM-  
506 CO<sub>2</sub> simulations described in the previous paragraph, except that non-CO<sub>2</sub> radiative forcing  
507 is abruptly set to zero in the year 2300. Note that this is different from setting emissions of  
508 non-CO<sub>2</sub> gases to zero because the finite atmospheric lifetime of these gases would lead to a  
509 gradual decline in their concentration and associated radiative forcing (except for aerosols,  
510 which have a very short atmospheric residence time). Similar to the PIEM-CO<sub>2</sub> runs, at-  
511 mospheric CO<sub>2</sub> declines after 2300 under all RCPs (Fig. 9). The rate of decrease is slightly  
512 larger than in the PIEM-CO<sub>2</sub> simulations due to the greater efficiency of the carbon sinks  
513 in a slightly cooler climate (i.e. a reduced climate-carbon cycle feedback). The surface tem-  
514 perature decreases abruptly around 2300, and more gradually thereafter, with a rate similar  
515 to that in the PIEM-CO<sub>2</sub> simulations. Accordingly, the warming commitment after 2300 is  
516 more negative than in the PIEM-CO<sub>2</sub> runs (Table 4). Note that the temperature response



517 in the simulations described here is different from that projected in simulations where all  
518 anthropogenic emissions are set to zero (Hare and Meinshausen 2006; Armour and Roe 2011;  
519 Matthews and Zickfeld 2012). In those simulations, temperature increases temporarily after  
520 elimination of emissions due to the removal of the negative radiative forcing from aerosols  
521 (Hare and Meinshausen 2006; Armour and Roe 2011; Matthews and Zickfeld 2012). In the  
522 RCPs used in the present study, the year-2300 non-CO<sub>2</sub> radiative forcing is dominated by  
523 the positive forcing from non-CO<sub>2</sub> greenhouse gases such that a removal of this forcing leads  
524 to a sudden cooling.

525 The sea level rise commitment in PIEM simulations is smaller than in PIEM-CO<sub>2</sub> simu-  
526 lations (Table 4), consistent with the more rapid decline in radiative forcing .

527 *e. Constant emission commitment*

528 The constant emission commitment simulations (CEM) differ from the simulations de-  
529 scribed previously in that CO<sub>2</sub> emissions are held constant at significant positive values after  
530 2300 in RCPs 4.5–8.5 (range of 0.8–6.4 PgCyr<sup>-1</sup>; Fig. 10). Since only a fraction of these  
531 CO<sub>2</sub> emissions is taken up by carbon sinks, atmospheric CO<sub>2</sub> increases again after 2300 (as  
532 opposed to remaining constant or decreasing as in the other commitment simulations). As  
533 a result, surface air temperature continues to increase, with a significant positive warming  
534 commitment after 2300 (Table 4). Thermosteric sea level also continues to rise after 2300,  
535 with the sea level rise between 2300 and 3000 being several factors larger than that realized  
536 by 2300 (Table 4).

537 The climate response in the RCP2.6 CEM simulation is very different from that under  
538 the higher RCPs: CO<sub>2</sub> emissions in the year 2300 are slightly negative in all models (-0.7 to  
539 -0.2 PgCyr<sup>-1</sup>), and holding emissions fixed at these values results in a continuing decrease  
540 in atmospheric CO<sub>2</sub>. Accordingly, global mean temperature continues to decrease, and sea  
541 level starts to fall between 2300 and 3000 in all models. The ensemble mean warming and  
542 sea level rise commitments are slightly more negative than to those in the RCP2.6 PIEM

543 commitment simulations (Table 4).

544 *f. Climate change reversibility*

545 To explore under which conditions the climate system can revert to its pre-industrial  
546 state, a set of “reversibility” simulations was carried out. These simulations were started  
547 from the year-3000 state of the constant composition commitment (CCO) simulations. Two  
548 simulations were performed with atmospheric CO<sub>2</sub> decreasing linearly to zero (“ramp”) over  
549 a period of 100 and 1000 years, respectively. These scenarios are highly idealized and are used  
550 for illustrative purpose only. Since the atmospheric CO<sub>2</sub> changes are externally prescribed,  
551 these simulations give insight into the reversibility of the physical climate system. A third  
552 simulation, in which atmospheric CO<sub>2</sub> is allowed to evolve freely after emissions are set to  
553 zero, is aimed at exploring the reversibility of changes in the coupled climate-carbon cycle  
554 system. It should be noted that non-CO<sub>2</sub> forcing after year 3000 is held fixed at slightly  
555 positive values and therefore the total forcing after ramp-down of atmospheric CO<sub>2</sub> to pre-  
556 industrial levels is different from zero.

557 With atmospheric CO<sub>2</sub> decreasing to pre-industrial levels over a period of 100 years,  
558 surface air temperature decreases rapidly at first (during the CO<sub>2</sub> ramp-down phase) and  
559 more slowly thereafter (Fig. 11). At the year 4000 surface air temperature is still higher than  
560 under 1851–1860 conditions (Table 5). This remaining warming 900 years after atmospheric  
561 CO<sub>2</sub> returned to pre-industrial levels can be explained by the thermal inertia of the climate  
562 system, which plays out both during periods of warming and cooling, and the (small) residual  
563 positive radiative forcing from non-CO<sub>2</sub> sources.

564 The thermosteric sea level rise trend is also reversed with decreasing atmospheric CO<sub>2</sub>.  
565 Rates of sea level fall, however, are slower than rates of cooling, and sea level is significantly  
566 higher than under pre-industrial conditions at year 4000 (Table 5). The thermohaline circu-  
567 lation exhibits a rapid strengthening in the ensemble mean during the CO<sub>2</sub> decrease phase,  
568 with the overturning first overshooting and then slowly converging to pre-industrial values.

569 Note that under RCP8.5 the thermohaline circulation is close to collapse in the Bern3D-LPJ  
570 model, but recovers after the ramp-down of atmospheric CO<sub>2</sub>.

571 In the simulations with a slower decrease of atmospheric CO<sub>2</sub> (over 1000 years), surface  
572 air temperature also starts to drop after the year 3000, but the cooling is more gradual  
573 than in the 100-year ramp-down experiment (Fig. 12). Also, the rate of cooling is lower  
574 during the first 500 years of the ramp-down than during the last 500 years. This nonlinear  
575 response can again be explained with the thermal inertia of the climate system: despite  
576 700 years of constant forcing (from 2300 to 3000) the climate system is still equilibrating  
577 with that forcing, and the associated warming commitment acts to offset the cooling due  
578 to decreasing CO<sub>2</sub> levels during the first few hundred years of the CO<sub>2</sub> ramp-down phase.  
579 Surface air temperature at 4000 is warmer than in the simulations with a 100-year ramp-  
580 down, particularly for the higher RCPs (Table 5).

581 In contrast to temperature, thermosteric sea level continues to rise for several centuries  
582 after CO<sub>2</sub> starts to decrease. For instance, ensemble mean sea level does not peak until the  
583 year 3200 under RCP6.0 and 3300 under RCP8.5. Year-4000 sea level rise is twice as high in  
584 these simulations than in the 100-year ramp-down experiments (Table 5). The thermohaline  
585 circulation recovers slowly at first and more rapidly towards the end of the CO<sub>2</sub> decrease  
586 phase. Under RCPs 4.5–8.5 the ensemble-mean overturning at year 4000 exceeds the pre-  
587 industrial value. Individual models deviate substantially from the ensemble-mean behavior.  
588 For instance, overturning in the Bern3D-LPJ model does not recover under declining CO<sub>2</sub>  
589 levels, but collapses completely around the year 3500.

590 In the third reversibility experiment, atmospheric CO<sub>2</sub> is allowed to evolve freely after the  
591 year 3000 (under zero CO<sub>2</sub> emissions). This simulation was performed by a subset of EMICs  
592 with an interactive carbon cycle only. It is similar to the pre-industrial CO<sub>2</sub>-emission com-  
593 mitment (PIEM-CO<sub>2</sub>) simulation, except that a 700-year CO<sub>2</sub> stabilization phase precedes  
594 the free-evolving-CO<sub>2</sub> phase (and emissions are exactly zero as opposed to slightly negative  
595 in the PIEM-CO<sub>2</sub> experiments). Following the cessation of CO<sub>2</sub> emissions, atmospheric CO<sub>2</sub>

596 declines due to CO<sub>2</sub> uptake by marine and terrestrial carbon sinks (Fig. 13). As discussed  
597 earlier for the PIEM-CO<sub>2</sub> experiments, surface air temperature remains approximately con-  
598 stant after elimination of CO<sub>2</sub> emissions, while sea level continues to rise. Compared to the  
599 reversibility experiments with CO<sub>2</sub> ramp-down, surface air temperature and sea level rise  
600 at 4000 are much higher in the free-evolving-CO<sub>2</sub> case (Table 5). Similarly to surface air  
601 temperature, the thermohaline circulation remains approximately constant after emissions  
602 cease. An exception is again the overturning in the Bern3D-LPJ model, which collapses  
603 completely by the year 3200.

604 EMICs with an interactive carbon cycle were used to diagnose the CO<sub>2</sub> emissions com-  
605 patible with the CO<sub>2</sub> concentration trajectories for the two reversibility experiments with  
606 CO<sub>2</sub> ramp-down (Fig. 14). The abrupt decrease of atmospheric CO<sub>2</sub> in the two experiments  
607 (Figs. 11a, 12a) requires emissions to become negative to close the CO<sub>2</sub> budget. Emissions  
608 are much more negative in the experiments with a fast (100-year) ramp-down than in those  
609 with a slower (1000-year) ramp-down, particularly under the higher RCPs. For each experi-  
610 ment, the larger the rate of atmospheric CO<sub>2</sub> decline, the more negative the diagnosed CO<sub>2</sub>  
611 emissions.

612 Negative emissions imply that the prescribed rate of atmospheric CO<sub>2</sub> decline exceeds  
613 the uptake capacity of the marine and terrestrial carbon sinks. In the 100-year ramp-down  
614 experiments, terrestrial carbon inventories decline strongly during the CO<sub>2</sub> decrease phase,  
615 and remain relatively stable thereafter in all models (Fig. 15). At year 4000, terrestrial  
616 carbon inventories are lower than at pre-industrial. The likely reason is the lag of surface  
617 air temperature relative to atmospheric CO<sub>2</sub>, such that the terrestrial biosphere is subject  
618 to higher temperatures despite a return to pre-industrial CO<sub>2</sub> conditions. Ocean carbon  
619 inventories also decline during the CO<sub>2</sub> ramp-down phase, although more gradually, and  
620 continue to decline until the end of the simulation in all models. At year 4000, ocean carbon  
621 inventories are higher than at pre-industrial in most models.

622 In the 1000-year ramp-down experiment, the decline in land carbon inventories in re-

623 sponse to declining CO<sub>2</sub> levels is more gradual and continues for the duration of the ramp-  
624 down (not shown). Ocean carbon inventories, on the other hand, continue to increase after  
625 the decline in atmospheric CO<sub>2</sub> in several models (exceptions are the UVic and UMD models).  
626 By year 3500, ocean carbon turns around and starts to decrease in all models. Continuing  
627 ocean carbon uptake at the beginning of the ramp-down phase offsets the carbon release  
628 from the terrestrial biosphere at first, such that diagnosed CO<sub>2</sub> emissions are only slightly  
629 negative. Diagnosed emissions become increasingly more negative towards the end of the  
630 ramp-down as both ocean and land release CO<sub>2</sub> into the atmosphere (Fig. 14b).

631 *g. Cumulative emissions compatible with temperature targets*

632 A last set of simulations was performed with the the UVic and Bern3D-LPJ EMICs to  
633 explore the cumulative emissions compatible with long-term temperature targets. These  
634 simulations used an inverse modelling approach, whereby CO<sub>2</sub> emissions compatible with  
635 prescribed temperature trajectories were diagnosed (Zickfeld et al. 2009). Fig. 16 displays  
636 the diagnosed cumulative emissions for temperature trajectories stabilizing at 1.5°C, 2°C,  
637 3°C and 4°C for the UVic and Bern3D-LPJ EMICs. The temperature trajectories prescribed  
638 to the two models are slightly different until the time of temperature stabilization (Fig. 16a).  
639 This does not affect the comparability of results, however, since we discuss the cumulative  
640 emissions since pre-industrial, and the climate response centuries after elimination of emis-  
641 sions is independent of the emission trajectory (Eby et al. 2009; Zickfeld et al. 2009, 2012).  
642 Model mean allowable cumulative emissions are 770 PgC, 1000 PgC, 1460 PgC and 1950 PgC  
643 for temperature targets of 1.5°C, 2°C, 3°C and 4°C, respectively. These estimates are slightly  
644 lower than the allowable cumulative emissions estimated with an earlier version of the UVic  
645 model (Zickfeld et al. 2009). The estimate for the 2°C target coincides with the value of  
646 1000 PgC from Allen et al. (2009), and is somewhat higher than the value calculated by  
647 Meinshausen et al. (2009), who assumed stronger forcing from non-CO<sub>2</sub> gases.

648 Allowable cumulative emissions at 2500 are slightly higher in the Bern3D-LPJ than in

649 the UVic model for the lower temperature targets (1.5–2°C), whereas they are lower for the  
650 highest temperature target (4°C). Allowable emissions consistent with temperature targets  
651 depend both on the physical and biogeochemical model response. For instance, the higher  
652 the climate sensitivity and/or the stronger the (positive) climate-carbon cycle feedback, the  
653 lower the amount of cumulative emissions consistent with a specified temperature target  
654 (Zickfeld et al. 2009). Both EMICs have a relatively high climate sensitivity and a high total  
655 carbon uptake sensitivity to temperature, but also a high total carbon uptake sensitivity to  
656 CO<sub>2</sub> (Eby et al. 2013, Tables 2, 4). The relative ordering of these sensitivities between the  
657 two models is time and scenario dependent (e.g. the equilibrium climate sensitivity is higher  
658 in UVic than Bern3D-LPJ at 2×CO<sub>2</sub>, but lower at 4×CO<sub>2</sub>) which may explain the change  
659 in ordering of allowable emissions with the level of temperature stabilization.

660 Matthews et al. (2009) proposed the Climate Carbon Response (CCR), defined as the  
661 ratio of temperature change to cumulative carbon emissions, as a metric for the combined  
662 physical and biogeochemical response of the climate system to CO<sub>2</sub> emissions. CCR has  
663 been suggested to be relatively insensitive to the emissions scenario, and approximately con-  
664 stant over time. Eby et al. (2013) calculated the CCR for eight EMICs with an interactive  
665 carbon cycle from an idealized 4×CO<sub>2</sub> experiment with a 1% CO<sub>2</sub> increase per year and  
666 noted that the CCR in the EMICS varies appreciably with time. At the time of CO<sub>2</sub> dou-  
667 bling, the CCR ranges from 1.4°C EgC<sup>-1</sup> to 2.5°C EgC<sup>-1</sup> (note that these numbers differ  
668 from those in Table 4 of Eby et al. (2013), which are taken at the time of CO<sub>2</sub> quadru-  
669 pling). The models' CCR can be inverted to compute the range of cumulative emissions  
670 consistent with temperature targets. Ensemble mean allowable cumulative emissions are  
671 830 PgC, 1100 PgC, 1650 PgC and 2200 PgC for temperature targets of 1.5°C, 2°C, 3°C and  
672 4°C, respectively (Fig. 17). Since the CCR was computed for cumulative emissions of about  
673 1000 PgC, CCR-based allowable emission estimates for temperature targets of 1.5–2°C are  
674 likely more accurate than those for the higher temperature targets. While the cumulative  
675 emissions estimated from the temperature tracking experiments and the CCR are very simi-

676 lar for the Bern3D-LPJ model, particularly for lower temperature targets, the CCR-derived  
677 estimates are considerably higher for the UVic model. The difference in the UVic model's  
678 allowable emissions estimates for the low temperature targets could be explained by a net  
679 positive radiative forcing from non-CO<sub>2</sub> sources in the temperature tracking simulations (not  
680 present in the idealized 4×CO<sub>2</sub> simulation from which the CCR was derived), which reduces  
681 the amount of allowable CO<sub>2</sub> emissions. Due to differences in forcing implementation, the  
682 non-CO<sub>2</sub> radiative forcing imbalance seems not to be present in the Bern3D-LPJ temper-  
683 ature tracking runs, such that the two allowable emissions estimates are very similar for  
684 low temperature targets. For higher targets, the discrepancy between the CCR-based and  
685 temperature-tracking-derived estimates is likely due to the time and scenario dependence of  
686 CCR.

## 687 4. Summary and Conclusions

688 We presented results from long-term climate projections with twelve EMICs. The first set  
689 of projections are climate change commitment simulations run until the year 3000. Three  
690 different types of climate commitment are considered: (i) constant composition, (ii) pre-  
691 industrial emission, and (iii) constant emission commitments. All commitment simulations  
692 follow common CO<sub>2</sub> concentration trajectories until the year 2300 - the four RCP scenarios  
693 (2.6, 4.5, 6.0 and 8.5) and their extensions. Climate projections to 2300 are consistent with  
694 results from AOGCMs, confirming that EMICs are well suited to complement simulations  
695 with more complex models. Simulated ensemble-mean surface air temperatures exceed the  
696 2°C target set by the Copenhagen Accord in all scenarios, except for the low emissions  
697 RCP2.6 scenario. Under this scenario, the model ensemble mean temperature peaks at  
698 1.7°C relative to pre-industrial, and returns to 1.3°C by 2300. The spread between models,  
699 however, is considerable, and peak warming in a few models exceeds the 2°C target.

700 EMICs simulate substantial surface air temperature and thermosteric sea level rise com-

701 mitment following stabilization of the atmospheric composition at year-2300 levels for RCPs  
702 4.5, 6.0 and 8.5. For these scenarios, the thermosteric sea level rise between years 2300 and  
703 3000 amounts to several times the sea level rise by the time of radiative forcing stabilization.  
704 Sea level rise due to thermal expansion still continues at the year 3000 under all scenarios  
705 considered. The Atlantic meridional overturning circulation is weakened temporarily under  
706 RCPs 2.6–6.0 and recovers to within 80% of the pre-industrial value several centuries after  
707 forcing stabilization. The MOC weakening is more persistent for RCP8.5, with one model  
708 close to a complete collapse in the year 3000.

709 EMICs with an interactive carbon cycle are used to diagnose the CO<sub>2</sub> emissions compati-  
710 ble with the CO<sub>2</sub> concentration pathways specified for the constant composition commitment  
711 simulations. Diagnosed cumulative emissions between 1850 and 3000 increase approximately  
712 linearly with atmospheric CO<sub>2</sub> for RCPs 2.6–6.0, but the increase becomes less than linear at  
713 higher radiative forcing. The year-3000 airborne fraction of cumulative emissions increases  
714 with increasing atmospheric CO<sub>2</sub>. The increasing airborne fraction is due largely to a de-  
715 crease in the ocean uptake fraction with higher radiative forcing. The model ensemble mean  
716 land uptake fraction is rather constant across RCP scenarios, but the CO<sub>2</sub> dependence varies  
717 strongly between models.

718 Elimination of anthropogenic CO<sub>2</sub> emissions after 2300 and constant year-2300 non-  
719 CO<sub>2</sub> radiative forcing results in slowly decreasing atmospheric CO<sub>2</sub> concentrations. At year  
720 3000 atmospheric CO<sub>2</sub> is still at more than half the year-2300 level in all EMICs for RCPs  
721 4.5–8.5, with the fraction increasing with RCP scenario. Surface air temperature remains  
722 nearly constant or decreases slightly in all EMICs, with 85–99% of the maximum warming  
723 still persisting in the year 3000 for RCPs 4.5–8.5. Sea level rise due to thermal expansion  
724 continues after elimination of CO<sub>2</sub> emissions in RCPs 4.5–8.5 and is comparable to the sea  
725 level rise between 1850 and 2300. At 3000, 700 years after anthropogenic CO<sub>2</sub> emissions are  
726 zeroed, sea level is still rising in several EMICs. If radiative forcing from non-CO<sub>2</sub> forcing  
727 agents is eliminated simultaneously with CO<sub>2</sub> emissions, the warming and thermosteric sea



728 level rise are slightly lower than in the simulations with elimination of CO<sub>2</sub> emissions alone,  
729 but still remain substantially higher in the year 3000 compared to pre-industrial.

730 The largest warming and thermosteric sea level rise commitment are simulated for the  
731 case with CO<sub>2</sub> emissions held fixed at year-2300 levels and constant year-2300 non-CO<sub>2</sub>  
732 radiative forcing. In response to anew increasing atmospheric CO<sub>2</sub> levels after 2300, surface  
733 air temperature and sea level continue to rise, with a substantial post-2300 commitment.

734 The climate change commitment associated with the low emissions scenario RCP 2.6  
735 differs from that of the higher RCPs. Due to the decline in atmospheric CO<sub>2</sub> and radiative  
736 forcing already before 2300, the warming and thermosteric sea level rise commitment after  
737 2300 are lower in this scenario. The difference is largest for the constant emissions com-  
738 mitment simulations, since year-2300 emissions are negative (as opposed to positive in the  
739 other scenarios). Accordingly, atmospheric CO<sub>2</sub> decreases after 2300, surface air temperature  
740 continues to cool, and sea level starts to fall.

741 Results of the climate change commitment simulations differ widely between EMICs, both  
742 in the physical and biogeochemical response. The difference in the response of the terrestrial  
743 carbon cycle to atmospheric CO<sub>2</sub> and climate is particularly large. Compared to an earlier  
744 EMIC intercomparison (Plattner et al. 2008), the range of carbon cycle responses appears to  
745 have even widened. This may be explained by the larger number of coupled climate-carbon  
746 cycle models included in the present model intercomparison, and the increase in model  
747 complexity since the Plattner et al. (2008) study. Most EMICs now include interactive  
748 representation of land use change emissions. One model includes representation of carbon  
749 release from permafrost and peatlands, while another includes nitrogen limitation. On the  
750 ocean side, several models now include representation of sediment processes. The large model  
751 spread suggests that continued efforts are needed to better understand the processes driving  
752 the response of land and ocean uptake to CO<sub>2</sub> and climate, and to better represent these  
753 processes in models.

754 If CO<sub>2</sub> emissions cease, and it is left to the natural carbon sinks to take up excess

755 CO<sub>2</sub>, atmospheric CO<sub>2</sub> declines only slowly, and climate change is largely irreversible on  
756 centennial to millennial timescales, as discussed above in the context of the pre-industrial  
757 emission commitment simulations. Two additional experiments were carried out by EMICs  
758 to explore the reversibility of the climate system in response to an artificial “ramp-down”  
759 of atmospheric CO<sub>2</sub> to pre-industrial levels (over 100 and 1000 years). Due to the large  
760 thermal inertia of the ocean, surface air temperature and sea level rise exhibit a substantial  
761 time lag relative to atmospheric CO<sub>2</sub>. 900 years after CO<sub>2</sub> is restored to pre-industrial levels,  
762 surface air temperature and particularly sea level are still considerably higher than under  
763 1851–1860 conditions. The thermohaline circulation strengthens rapidly during the CO<sub>2</sub>  
764 decrease phase, first overshooting and then slowly converging to the pre-industrial value. If  
765 atmospheric CO<sub>2</sub> is returned to pre-industrial levels more slowly (over 1000 years), surface  
766 air temperature also cools more slowly, and sea level continues to rise for several centuries  
767 before starting to fall. The model ensemble mean thermohaline circulation recovers slowly  
768 at first and more rapidly towards the end of the CO<sub>2</sub> decrease phase. The ramp-down of  
769 CO<sub>2</sub> to pre-industrial levels over 100–1000 years requires large negative emissions, i.e. net  
770 removal of CO<sub>2</sub> from the atmosphere, which are likely unrealistic with technologies currently  
771 available to capture CO<sub>2</sub> from the atmosphere (McGlashan et al. 2012).

772 In summary, results from the commitment and reversibility simulations suggest that it  
773 is very difficult to revert from a given level of warming on timescales relevant to human  
774 activities, even after complete elimination of emissions. Reversing global warming may  
775 be desirable if climate change exceeds adaptive capacities of natural and human systems.  
776 Our results suggest that significant negative emissions have the potential to reverse global  
777 warming but whether CO<sub>2</sub> capture technology is feasible at the necessary scale is debatable.

778 Using an inverse modelling approach, two EMICs (Bern3D-LPJ, UVic) estimated the  
779 cumulative CO<sub>2</sub> emissions (“CO<sub>2</sub> budget”) compatible with long-term global mean temper-  
780 ature stabilization targets. Cumulative emissions between pre-industrial and the year 2500  
781 are similar between the two models and amount to a mean value of 1000 PgC for the 2°C.

782 A somewhat higher model ensemble mean estimate is derived based on the Climate Carbon  
783 Response (CCR; Matthews et al. (2009)) computed for EMICs with an interactive carbon  
784 cycle. As cumulative CO<sub>2</sub> emissions from fossil fuels and land use up to today amount to  
785 about 500 PgC, the remaining CO<sub>2</sub> budget consistent with the 2°C target is about 500 PgC,  
786 assuming that the radiative forcing of non-CO<sub>2</sub> greenhouse gases continues to be compen-  
787 sated by negative aerosol forcing, as has been approximately the case in the past. The results  
788 of this model intercomparison therefore support the conclusions from previous studies that  
789 it is still possible in theory to meet the 2°C target, but leeway is getting tight, particularly  
790 in the face of socio-economic and technological inertia.

791 *Acknowledgments.*

792 KZ and AJW acknowledge support from the National Science and Engineering Research  
793 Council (NSERC) Discovery Grant Program. AJW acknowledges support from NSERC's  
794 G8 Research Councils Initiative on Multilateral Research Funding Program. AVE and IIM  
795 were supported by the the President of Russia grant 5467.2012.5, by the Russian Founda-  
796 tion for Basic Research, and by the programs of the Russian Academy of Sciences. EC, TF,  
797 HG and GPB acknowledge support from the Belgian Federal Science Policy Office. FJ, RS  
798 and MS acknowledges support by the Swiss National Science Foundation and by the Euro-  
799 pean Project CARBOCHANGE (grant 264879) which received funding from the European  
800 Commissions Seventh Framework Programme (FP7/20072013). PBH and NRE acknowledge  
801 support from EU FP7 grant ERMITAGE no. 265170.

## REFERENCES

804 Allen, M. R., D. J. Frame, C. Huntingford, C. D. Jones, J. A. Lowe, M. Meinshausen,  
805 and N. Meinshausen, 2009: Warming caused by cumulative carbon emissions towards the  
806 trillionth tonne. *Nature*, **458**, 1163–1166.

807 Archer, D. and V. Brovkin, 2008: The millennial atmospheric lifetime of anthropogenic CO<sub>2</sub>.  
808 *Clim. Change*, **90** (3), 283–297, doi:10.1007/s10584-008-9413-1.

809 Archer, D., et al., 2009: Atmospheric Lifetime of Fossil Fuel Carbon Dioxide. *Annu. Rev.*  
810 *Earth Planet. Sci.*, **37**, 117–134, doi:10.1146/annurev.earth.031208.100206.

811 Armour, K. C. and G. H. Roe, 2011: Climate commitment in an uncertain world. *Geophys.*  
812 *Res. Lett.*, **38**, doi:10.1029/2010GL045850.

813 Arora, V. K., J. F. Scinocca, G. J. Boer, J. R. Christian, K. L. D. G. M. Flato, V. V.  
814 Kharin, W. G. Lee, and W. J. Merryfield, 2011: Carbon emission limits required to satisfy  
815 future representative concentration pathways of greenhouse gases. *Geophys. Res. Lett.*, **38**,  
816 L05 805, doi:10.1029/2010GL046270.

817 Azar, C., K. Lindgren, E. Larson, and K. Möllersten, 2006: Carbon Capture and Storage  
818 From Fossil Fuels and Biomass Costs and Potential Role in Stabilizing the Atmosphere.  
819 *Clim. Change*, **47**, 47–79.

820 Boucher, O., et al., 2012: Reversibility in an earth system model in response to CO<sub>2</sub> con-  
821 centration changes. *Env. Res. Lett.*, **7**, doi:10.1088/1748-9326/7/2/024013.

822 Church, J. A., et al., 2013: Sea Level Change. *Climate Change 2013: The Physical Science*  
823 *Basis, Contribution of WG I to the Fourth Assessment Report of the IPCC*, T. Stocker

824 and D. Qin, Eds., Cambridge University Press, Cambridge, UK and New York, USA, In  
825 Preparation.

826 Collins, M., et al., 2013: Long-term Climate Change: Projections, Commitments and Ir-  
827 reversibility. *Climate Change 2013: The Physical Science Basis, Contribution of WG I*  
828 *to the Fourth Assessment Report of the IPCC*, T. Stocker and D. Qin, Eds., Cambridge  
829 University Press, Cambridge, UK and New York, USA, In Preparation.

830 Denman, K. L., et al., 2007: Coupling between changes in the climate system and biogeo-  
831 chemistry. *Climate Change 2007: The Physical Science Basis, Contribution of WG I to*  
832 *the Fourth Assessment Report of the IPCC*, S. Solomon, D. Qin, and M. Manning, Eds.,  
833 Cambridge University Press, Cambridge, UK and New York, USA, 499–587.

834 Eby, M., K. Zickfeld, A. Montenegro, D. Archer, K. J. Meissner, and A. J. Weaver, 2009:  
835 Lifetime of anthropogenic climate change: millennial time scales of potential CO<sub>2</sub> and  
836 temperature perturbations. *J. Clim.*, **22**, 2501–2511.

837 Eby, M., et al., 2013: Historical and idealized climate model experiments: An EMIC inter-  
838 comparison. *Climate of the Past*, in revision.

839 Eliseev, A. V. and I. I. Mokhov, 2011: Uncertainty of climate response to natural and  
840 anthropogenic forcings due to different land use scenarios. *Adv. Atmos. Sci.*, **28** (5),  
841 1215–1232, doi:10.1007/s00376-010-0054-8.

842 Friedlingstein, P., et al., 2006: Climate-carbon cycle feedback analysis: Results from the  
843 C4MIP model intercomparison. *J. Clim.*, **19**, 3337–3353.

844 Froelicher, T. and F. Joos, 2010: Reversible and irreversible impacts of greenhouse gas  
845 emissions in multi-century projections with a comprehensive climate-carbon model. *Clim.*  
846 *Dyn.*, **35** (7–8), 1439–1459, doi:10.1007/s00382-009-0727-0.

847 GEA, 2012: *Global Energy Assessment- Toward a Sustainable Future*. Cambridge University  
848 Press, Cambridge, UK and New York, NY, USA and the International Institute for Applied  
849 Systems Analysis, Laxenburg, Austria.

850 Gillett, N., V. Arora, K. Zickfeld, S. Marshall, and W. Merryfield, 2011: Ongoing climate  
851 change following a complete cessation of carbon dioxide emissions. *Nat. Geosci.*, **4**, 83–87.

852 Goosse, H., et al., 2010: Description of the Earth system model of intermediate com-  
853 plexity LOVECLIM version 1.2. *Geosci. Model Dev.*, **3** (2), 603–633, doi:10.5194/  
854 gmd-3-603-2010.

855 Hansen, J., G. Russell, A. Lacis, I. Fung, D. Rind, and P. Stone, 1985: Climate response-  
856 times - dependence on climate sensitivity and ocean mixing. *Science*, **229** (4716), 857–859,  
857 doi:10.1126/science.229.4716.857.

858 Hare, B. and M. Meinshausen, 2006: How much warming are we committed to and how  
859 much can be avoided? *Clim. Change*, **75** (1-2), 111–149, doi:10.1007/s10584-005-9027-9.

860 Held, I. M., M. Winton, K. Takahashi, T. Delworth, F. Zeng, and G. K. Vallis, 2010: Probing  
861 the Fast and Slow Components of Global Warming by Returning Abruptly to Preindustrial  
862 Forcing. *J. Clim.*, **23** (9), 2418–2427, doi:10.1175/2009JCLI3466.1.

863 Holden, P. B., N. R. Edwards, D. Gerten, and S. Schaphoff, 2013: A model based constraint  
864 on CO<sub>2</sub> fertilisation. *Biogeosci.*, **10**, 339–355, doi:10.5194/bg-10-339-2013.

865 Keith, D., M. Ha-Duong, and J. Stolaroff, 2006: Climate strategy with CO<sub>2</sub> capture from  
866 the air. *Clim. Change*, **74** (1-3), 17–45, doi:10.1007/s10584-005-9026-x.

867 Lowe, J. A., C. Huntingford, S. C. B. Raper, C. D. Jones, S. K. Liddicoat, and L. K. Gohar,  
868 2009: How difficult is it to recover from dangerous levels of global warming? *Environ.*  
869 *Res. Lett.*, **4** (1), doi:10.1088/1748-9326/4/1/014012.

870 MacDougall, A., C. Avis, and A. Weaver, 2012: Significant existing commitment to warming  
871 from the permafrost carbon feedback. *Nat. Geosci.*, **5**, 719–721.

872 Matsumoto, K., K. S. Tokos, A. R. Price, and S. J. Cox, 2008: First description of the  
873 Minnesota Earth System Model for Ocean biogeochemistry (MESMO 1.0). *Geosci. Model*  
874 *Dev.*, **1** (1), 1–15.

875 Matthews, H. D. and K. Caldeira, 2008: Stabilizing climate requires near-zero emissions.  
876 *Geophys. Res. Lett.*, **35** (4), L04705, doi:10.1029/2007GL032388.

877 Matthews, H. D., N. P. Gillett, P. A. Stott, and K. Zickfeld, 2009: The proportionality of  
878 global warming to cumulative carbon emissions. *Nature*, **459**, 829–832.

879 Matthews, H. D. and A. J. Weaver, 2010: Committed climate warming. *Nat. Geosci.*, **3** (3),  
880 142–143, doi:10.1038/ngeo813.

881 Matthews, H. D. and K. Zickfeld, 2012: Climate response to zeroed emissions of greenhouse  
882 gases and aerosols. *Nat. Clim. Chang.*, **2** (5), 338–341, doi:10.1038/NCLIMATE1424.

883 McGlashan, N., N. Shah, B. Caldecott, and M. Workman, 2012: High-level techno-economic  
884 assessment of negative emissions technologies. *Process Safety and Environmental Protec-*  
885 *tion*, **90**, 501–510.

886 Meehl, G., W. Washington, W. Collins, J. Arblaster, A. Hu, L. Buja, W. Strand, and  
887 H. Teng, 2005: How much more global warming and sea level rise? *Science*, **307** (5716),  
888 1769–1772, doi:10.1126/science.1106663.

889 Meehl, G., et al., 2007: Global climate projections. *Climate Change 2007: The Physical*  
890 *Science Basis, Contribution of WG I to the Fourth Assessment Report of the IPCC*,  
891 S. Solomon, D. Qin, and M. Manning, Eds., Cambridge University Press, Cambridge,  
892 UK and New York, USA, 747–845.

893 Meinshausen, M., N. Meinshausen, W. Hare, S. C. B. Raper, K. Frieler, R. Knutti, D. Frame,  
894 and M. Allen, 2009: Greenhouse-gas emission targets for limiting global warming to 2°C.  
895 *Nature*, **458**, 1158–1162.

896 Meinshausen, M., S. C. B. Raper, and T. M. L. Wigley, 2011a: Emulating coupled  
897 atmosphere-ocean and carbon cycle models with a simpler model, MAGICC6-Part  
898 1: Model description and calibration. *Atmos. Chem. Phys.*, **11** (4), 1417–1456, doi:  
899 10.5194/acp-11-1417-2011.

900 Meinshausen, M., et al., 2011b: The RCP greenhouse gas concentrations and their extensions  
901 from 1765 to 2300. *Clim. Change*, **109** (1-2, SI), 213–241, doi:10.1007/s10584-011-0156-z.

902 Montenegro, A., V. Brovkin, M. Eby, D. E. Archer, and A. J. Weaver, 2007: Long term fate  
903 of anthropogenic carbon. *Geophys. Res. Lett.*, **34**, L19 703, doi:10.1029/2007GL031 018.

904 Montoya, M., A. Griesel, A. Levermann, J. Mignot, M. Hofmann, A. Ganopolski, and  
905 S. Rahmstorf, 2005: The earth system model of intermediate complexity CLIMBER-  
906 3 alpha. Part 1: description and performance for present-day conditions. *Clim. Dyn.*,  
907 **25** (2-3), 237–263, doi:10.1007/s00382-005-0044-1.

908 Morice, C. P., J. J. Kennedy, N. A. Rayner, and P. D. Jones, 2013: Quantifying uncertainties  
909 in global and regional temperature change using an ensemble of observational estimates:  
910 The hadcrut4 dataset. *J. Geophys. Res.*, doi:10.1029/2011JD017187, in press.

911 Moss, R. H., et al., 2010: The next generation of scenarios for climate change research and  
912 assessment. *Nature*, **463** (7282), 747–756, doi:{10.1038/nature08823}.

913 Nusbaumer, J. and K. Matsumoto, 2008: Climate and carbon cycle changes under the  
914 overshoot scenario. *Global and Planetary Change*, **62**, 164–172.

915 Petoukhov, V., A. Ganopolski, V. Brovkin, M. Claussen, A. Eliseev, C. Kubatzki, and  
916 S. Rahmstorf, 2000: CLIMBER-2: a climate system model of intermediate complexity.



917 Part I: model description and performance for present climate. *Clim. Dyn.*, **16** (1), 1–17,  
918 doi:10.1007/PL00007919.

919 Plattner, G.-K., et al., 2008: Long-term climate commitments projected with climate-carbon  
920 cycle models. *J. Clim.*, **21**, 2721–2751.

921 Rhein, M., et al., 2013: Observations: Ocean. *Climate Change 2013: The Physical Science*  
922 *Basis, Contribution of WG I to the Fourth Assessment Report of the IPCC*, T. Stocker  
923 and D. Qin, Eds., Cambridge University Press, Cambridge, UK and New York, USA, In  
924 Preparation.

925 Ritz, S. P., T. F. Stocker, and F. Joos, 2011: A Coupled Dynamical Ocean-Energy  
926 Balance Atmosphere Model for Paleoclimate Studies. *J. Clim.*, **24** (2), 349–375, doi:  
927 10.1175/2010JCLI3351.1.

928 Sabine, C. L., et al., 2004: The oceanic sink for anthropogenic CO<sub>2</sub>. *Science*, **305**, 367–371.

929 Shaffer, G., S. M. Olsen, and J. O. P. Pedersen, 2008: Presentation, calibration and validation  
930 of the low-order, DCESS Earth System Model (Version 1). *Geosci. Model Dev.*, **1** (1), 17–  
931 51.

932 Sokolov, A., et al., 2005: The MIT Integrated Global System Model (IGSM) Version 2:  
933 Model Description and Baseline Evaluation. Tech. rep., MIT.

934 Solomon, S., J. S. Daniel, T. J. Sanford, D. M. Murphy, G.-K. Plattner, R. Knutti, and  
935 P. Friedlingstein, 2010: Persistence of climate changes due to a range of greenhouse gases.  
936 *Proc. Natl. Acad. Sci. U. S. A.*, **107** (43), 18 354–18 359, doi:10.1073/pnas.1006282107.

937 Solomon, S., G.-K. Plattner, R. Knutti, and P. Friedlingstein, 2009: Irreversible climate  
938 change due to carbon dioxide emissions. *Proc. Natl. Acad. Sci. U. S. A.*, **106** (6), 1704–  
939 1709.

- 940 Stocker, B. D., K. Strassmann, and F. Joos, 2011: Sensitivity of holocene atmospheric CO<sub>2</sub>  
941 and the modern carbon budget to early human land use: analyses with a process-based  
942 model. *Biogeosci.*, **8**, 69–88.
- 943 Tachiiri, K., J. C. Hargreaves, J. D. Annan, A. Oka, A. Abe-Ouchi, and M. Kawamiya,  
944 2010: Development of a system emulating the global carbon cycle in Earth system models.  
945 *Geosci. Model Dev.*, **3** (2), 365–376, doi:10.5194/gmd-3-365-2010.
- 946 Taylor, K. E., R. J. Stouffer, and G. A. Meehl, 2008: A summary of the CMIP5 experiment  
947 design. Tech. rep.
- 948 Tsutsui, J., Y. Yoshida, D.-H. Kim, H. Kibata, K. Nishizawa, N. Nakashiki, and K. Mu-  
949 rayama, 2007: Long-term climate response to stabilized and overshoot anthropogenic  
950 forcings beyond the twenty first century. *Clim. Dyn.*, **28**, 199–214.
- 951 Weaver, A. J., et al., 2001: The UVic Earth System Climate Model: Model description,  
952 climatology, and applications to past, present and future climates. *Atmos.-Ocean*, **39**,  
953 361–428.
- 954 Wigley, T., 2005: The climate change commitment. *Science*, **307** (5716), 1766–1769, doi:  
955 10.1126/science.1103934.
- 956 Yoshida, Y., K. Maruyama, J. Tsutsui, N. Nakashiki, F. O. Bryan, M. Blackmon, B. A.  
957 Boville, and R. D. Smith, 2005: Multi-century ensemble global warming projections using  
958 the Community Climate System Model (CCSM3). *J. Earth Simulator*, **3**, 2–10.
- 959 Zeng, N., H. Qian, E. Munoz, and R. Iacono, 2004: How strong is carbon cycle-  
960 climate feedback under global warming? *Geophys. Res. Lett.*, **31** (L20203), doi:  
961 10.1007/s00376-010-0054-8.
- 962 Zickfeld, K., V. K. Arora, and N. P. Gillett, 2012: Is the climate response to carbon emissions  
963 path dependent? *Geophys. Res. Lett.*, **39**, L05 703, doi:10.1029/2011GL050205.

964 Zickfeld, K., M. Eby, H. Matthews, and A. J. Weaver, 2009: Setting cumulative emissions  
965 targets to reduce the risk of dangerous climate change. *Proc. Natl. Acad. Sci. U.S.A.*,  
966 **106 (38)**, 16 129–16 134.

## List of Tables

- 967
- 968 1 Model experiments. 40
- 969 2 Changes in climate and carbon cycle variables from EMIC historical simula-  
970 tions and observations. Shown are the warming over the 20<sup>th</sup> century ( $\Delta T$ ),  
971 the rate of thermosteric sea level rise averaged over 1971–2010 ( $SLR_{th}$ ), the  
972 carbon fluxes averaged over 1990–1999 and cumulative fluxes from 1800 to  
973 1994.  $Land_{LUC}$  are land-use change fluxes from simulations with land-use  
974 forcing only (see Eby et al. (2013)).  $Land_{RES}$  is the residual land flux, which  
975 is derived as the difference between the land flux from the historical simula-  
976 tion with all forcings and  $Land_{LUC}$ . Carbon fluxes are positive when directed  
977 into the atmosphere. Observations-based estimates are from Morice et al.  
978 (2013) for the 20<sup>th</sup> century warming, Rhein et al. (2013, Table 3.1) for 1971–  
979 2010 thermal expansion, Denman et al. (2007, Table 7.1) for the 1990s carbon  
980 fluxes and Sabine et al. (2004) for the cumulative carbon fluxes. 41
- 981 3 Global mean warming and thermal expansion relative to the 1986–2005 ref-  
982 erence period for selected time periods and four RCPs. CMIP5 surface air  
983 temperature anomalies (Collins et al. 2013, Table 12.2) and thermal expan-  
984 sion (Church et al. 2013, Table 13.5) are shown for comparison. Listed are  
985 the model ensemble mean and the minimum and maximum values from the  
986 model distribution (in brackets). For CMIP5 thermal expansion the values  
987 in brackets span the likely range. EMIC year 2981–3000 values are from the  
988 constant-composition (CCO) simulations. 42
- 989 4 Projected global mean warming and thermosteric sea level rise between 2300  
990 and 3000 in constant-emissions (CEM), constant-composition (CCO), pre-  
991 industrial CO<sub>2</sub>-emissions (PIEM-CO<sub>2</sub>) and pre-industrial emission (PIEM)  
992 commitment simulations. Given are model ensemble means and model ranges  
993 (in brackets). 43

994 5 Warming and thermosteric sea level in 3991–4000 relative to 1851–1860 for  
995 climate reversibility simulations with a 100-year ramp-down of atmospheric  
996 CO<sub>2</sub> after the year 3000 (REa), a 1000-year ramp-down of atmospheric CO<sub>2</sub>  
997 (REb) and freely evolving CO<sub>2</sub> (REc). Given are model ensemble means and  
998 model ranges (in brackets).

44

TABLE 1. Model experiments.

Label	Simulation	Timeframe	CO <sub>2</sub>	Forcing	Non-CO <sub>2</sub> GHGs	# Models
HIST	Historical	1850–2005	CMIP5 concentration		CMIP5 forcing	12
RCP	RCPs and extensions	2006–2300	CMIP5 concentration		CMIP5 forcing	12
CCO	Const. composition commit.	2301–3000	Const. year-2300 conc.		Const. year-2300 forc.	12
PIEM-CO <sub>2</sub>	PI CO <sub>2</sub> emission commit.	2301–3000	Const. 1840–1850 emissions		Const. year-2300 forc.	7
PIEM	PI emission commit.	2301–3000	Const. 1840–1850 emissions		Const. 1840–1850 forc.	7
CEM	Const. emission commit.	2301–3000	Const. 2290–2300 emissions		Const. year-2300 forc.	7
REa	Reversibility a	3001–4000	Lin. decrease in conc. for 100 yrs		Const. year-2300 forc.	11
REb	Reversibility b	3001–4000	Lin. decrease in conc. for 1000 yrs		Const. year-2300 forc.	11
REc	Reversibility c	3001–4000	Zero emissions		Const. year-2300 forc.	7
TTR	Temperature tracking	2005–2500	Diagnosed		Lin. decrease to zero by 2300	2

TABLE 2. Changes in climate and carbon cycle variables from EMIC historical simulations and observations. Shown are the warming over the 20<sup>th</sup> century ( $\Delta T$ ), the rate of thermosteric sea level rise averaged over 1971–2010 ( $SLR_{th}$ ), the carbon fluxes averaged over 1990–1999 and cumulative fluxes from 1800 to 1994.  $Land_{LUC}$  are land-use change fluxes from simulations with land-use forcing only (see Eby et al. (2013)).  $Land_{RES}$  is the residual land flux, which is derived as the difference between the land flux from the historical simulation with all forcings and  $Land_{LUC}$ . Carbon fluxes are positive when directed into the atmosphere. Observations-based estimates are from Morice et al. (2013) for the 20<sup>th</sup> century warming, Rhein et al. (2013, Table 3.1) for 1971–2010 thermal expansion, Denman et al. (2007, Table 7.1) for the 1990s carbon fluxes and Sabine et al. (2004) for the cumulative carbon fluxes.

Model	$\Delta T$ (°C)	$SLR_{th}$ (mm/yr)	1990s carbon fluxes				Cumulative fluxes 1800–1994		
			$Land_{LUC}$ (PgC/yr)	$Land_{RES}$ (PgC/yr)	Ocean (PgC/yr)	Emissions (PgC/yr)	Land (PgC)	Ocean (PgC)	Emissions (PgC)
Bern3D-LPJ	0.57	0.81	0.7	-0.8	-1.8	5.2	108	-104	156
CLIMBER-2	0.91	1.66	–	–	–	–	–	–	–
CLIMBER-3	0.91	1.55	–	–	–	–	–	–	–
DCESS	0.84	1.10	0.3	-0.9	-1.8	5.7	4	-102	258
GENIE	1.00	1.05	0.5	-1.4	-2.1	6.1	21	-114	251
IAPRASC	0.80	–	–	–	–	–	–	–	–
IGSM	0.70	0.56	0.3	-0.7	-2.2	5.9	43	-122	237
LOVECLIM	0.38	0.67	–	–	–	–	–	–	–
MESMO	1.15	1.13	–	-0.6	-1.9	5.9	-28	-102	305
MIROC-lite-LCM	0.70	0.92	–	-0.1 <sup>a</sup>	-1.6	5.4	108 <sup>b</sup>	-86 <sup>b</sup>	140 <sup>b</sup>
UMD	0.79	1.56	–	-0.6	-2.4	6.2	-51	-136	347
UVic	0.75	1.43	1.3	-1.2	-2.0	5.2	24	-112	248
EMIC mean <sup>c</sup>	0.78 <sup>d</sup>	1.13	0.6	-1.0	-1.9 <sup>d</sup>	5.6	40	-111	230
EMIC range <sup>c</sup>	0.38 to 1.15	0.56 to 1.66	0.3 to 1.3	-1.4 to -0.7	-2.2 to -1.6	5.2 to 6.1	4 to 108	-122 to -102	156 to 258
Observed	0.73	0.8	1.6	-2.6	-2.2	6.4	39	-118	244
Uncertainty		0.5 to 1.1	0.5 to 2.7	-4.3 to -0.9	-2.6 to -1.8	6.0 to 6.8	11 to 67	-137 to -99	224 to 264

<sup>a</sup>Land-use change fluxes could not be diagnosed for this model because of the lack of a historical simulation with land-use change forcing only.

<sup>b</sup>Cumulative fluxes for this model are for 1851–1994.

<sup>c</sup>The MESMO and UMD models were excluded from the EMIC mean and range for the carbon cycle variables because they did not simulate land use change fluxes. Only the total land flux is reported for these models. The MIROC-lite-LCM model was excluded from the EMIC mean and range for the 1800–1994 cumulative fluxes because no carbon flux data was available prior to 1851.

<sup>d</sup>These values differ slightly from those reported in Eby et al. (2013) because of a different subset of EMICs included in the calculation.

TABLE 3. Global mean warming and thermal expansion relative to the 1986–2005 reference period for selected time periods and four RCPs. CMIP5 surface air temperature anomalies (Collins et al. 2013, Table 12.2) and thermal expansion (Church et al. 2013, Table 13.5) are shown for comparison. Listed are the model ensemble mean and the minimum and maximum values from the model distribution (in brackets). For CMIP5 thermal expansion the values in brackets span the likely range. EMIC year 2981–3000 values are from the constant-composition (CCO) simulations.

Scenario	2081–2100		2281–2300		2981–3000
	EMIC	CMIP5	EMIC	CMIP5	EMIC
Warming (°C)					
RCP2.6	1.0 (0.6, 1.4)	1.0 (0.0, 2.0)	0.6 (0.3, 1.0)	0.7 (0.3, 1.4)	0.6 (0.3, 1.1)
RCP4.5	1.7 (0.9, 2.4)	1.8 (1.0, 2.8)	2.2 (1.3, 3.0)	2.6 (1.7, 3.9)	2.5 (1.7, 3.5)
RCP6.0	2.1 (1.1, 2.8)	2.3 (1.5, 3.2)	3.3 (1.9, 4.5)	4.2 (3.6, 4.9)	3.8 (2.6, 5.0)
RCP8.5	3.1 (1.6, 4.1)	3.7 (2.5, 5.0)	7.0 (3.8, 8.9)	8.6 (5.0, 14.1)	7.8 (4.7, 9.8)
Thermal expansion (m)					
RCP2.6	0.14 (0.05, 0.20)	0.14 (0.10, 0.18)	0.22 (0.06, 0.37)	–	0.33 (0.09, 0.68)
RCP4.5	0.18 (0.09, 0.26)	0.19 (0.14, 0.23)	0.45 (0.17, 0.69)	–	0.82 (0.29, 1.64)
RCP6.0	0.20 (0.10, 0.29)	0.19 (0.15, 0.24)	0.62 (0.26, 0.95)	–	1.20 (0.47, 2.29)
RCP8.5	0.27 (0.13, 0.38)	0.27 (0.21, 0.33)	1.17 (0.64, 1.66)	–	2.48 (1.24, 4.31)



TABLE 4. Projected global mean warming and thermosteric sea level rise between 2300 and 3000 in constant-emissions (CEM), constant-composition (CCO), pre-industrial CO<sub>2</sub>-emissions (PIEM-CO<sub>2</sub>) and pre-industrial emission (PIEM) commitment simulations. Given are model ensemble means and model ranges (in brackets).

Scenario	CEM	CCO	PIEM-CO <sub>2</sub>	PIEM
Warming commitment (°C)				
RCP2.6	-0.8 (-1.0, -0.4)	0.0 (-0.1, 0.1)	-0.4 (-0.7, 0.4)	-0.8 (-1.2, 0.4)
RCP4.5	0.8 (0.5, 1.3)	0.3 (0.0, 0.6)	-0.5 (-1.0, 0.3)	-1.2 (-1.8, 0.3)
RCP6.0	1.1 (0.7, 1.4)	0.4 (0.0, 0.9)	-0.5 (-1.2, 0.4)	-1.2 (-2.0, 0.4)
RCP8.5	1.3 (0.7, 1.7)	0.7 (0.0,1.2)	-0.1 (-0.7, 0.6)	-1.3 (-2.3, 0.6)
Thermal expansion commitment (m)				
RCP2.6	-0.04 (-0.10, 0.02)	0.11 (0.03, 0.32)	0.04 (-0.02, 0.15)	-0.03 (-0.09, 0.15)
RCP4.5	0.40 (0.16, 0.83)	0.38 (0.12, 0.95)	0.18 (0.02, 0.49)	0.08 (-0.08, 0.34)
RCP6.0	0.60 (0.24, 1.19)	0.57 (0.20, 1.34)	0.29 (0.04, 0.69)	0.16 (-0.07, 0.47)
RCP8.5	1.30 (0.41, 2.84)	1.31 (0.38, 2.64)	0.97 (0.22, 2.37)	0.66 (0.03, 1.69)

TABLE 5. Warming and thermosteric sea level in 3991–4000 relative to 1851–1860 for climate reversibility simulations with a 100-year ramp-down of atmospheric CO<sub>2</sub> after the year 3000 (REa), a 1000-year ramp-down of atmospheric CO<sub>2</sub> (REb) and freely evolving CO<sub>2</sub> (REc). Given are model ensemble means and model ranges (in brackets).

Scenario	Warming (°C)		
	REa	REb	REc
RCP2.6	0.4 (0.1,0.5)	0.5 (0.1,0.7)	1.3 (0.7,1.8)
RCP4.5	0.7 (0.5,0.9)	1.1 (0.6,1.4)	3.2 (2.2,4.0)
RCP6.0	0.9 (0.6,1.3)	1.4 (0.7,1.9)	4.5 (3.4,5.3)
RCP8.5	2.0 (1.1,4.3)	3.1 (1.5,4.6)	8.9 (6.7,10.2)
Thermal expansion (m)			
RCP2.6	0.2 (0.05,0.4)	0.3 (0.1,0.7)	0.4 (0.1,0.8)
RCP4.5	0.3 (0.1,0.9)	0.5 (0.2,1.5)	0.8 (0.4,1.6)
RCP6.0	0.4 (0.1,1.1)	0.8 (0.3,2.0)	1.2 (0.6,2.4)
RCP8.5	0.8 (0.2,1.9)	1.9 (0.5,3.5)	2.9 (1.3,6.3)

## 999 List of Figures

- 1000 1 Time evolution of atmospheric CO<sub>2</sub> between 2006 and 2300 for the four RCP  
1001 scenarios and their extensions (RCP database version 2.0, [https://www.iiasa.ac.at/web-](https://www.iiasa.ac.at/web-apps/tnt/RcpDb/)  
1002 [apps/tnt/RcpDb/](https://www.iiasa.ac.at/web-apps/tnt/RcpDb/)). 50
- 1003 2 Constant composition commitment. Time evolution of physical climate vari-  
1004 ables for four RCP scenarios: (a) Surface air temperature change, (b) Fraction  
1005 of realized warming (calculated as the ratio of warming at any time to the  
1006 warming averaged over 2981–3000), (c) Ocean thermal expansion, (d) Atlantic  
1007 overturning index, defined as the maximum value of the overturning stream-  
1008 function in the North Atlantic. Anomalies are relative to 1986–2005. Shown  
1009 are the model ensemble averages (thick solid lines), the ranges spanned by  
1010 all models (shaded domains, delimited by thin solid lines), and the range in  
1011 the year 3000 (vertical bars on right hand side). Data were smoothed using a  
1012 ten-year moving average. 51
- 1013 3 RCP2.6 constant composition commitment simulations. (a) Surface air tem-  
1014 perature change, (b) Ocean thermal expansion. Anomalies are relative to  
1015 1986–2005. Data in panel (a) were smoothed using a ten-year moving average. 52
- 1016 4 Changes in carbon inventories in RCP2.6 constant composition commitment  
1017 simulations for eight EMICs with an interactive carbon cycle. (a) CO<sub>2</sub> emis-  
1018 sions, (b) Cumulative CO<sub>2</sub> emissions since 1850, (c) Atmospheric CO<sub>2</sub> con-  
1019 centration, (d) Airborne fraction of cumulative emissions, (e) Land uptake  
1020 since 1850, (f) Fraction of cumulative emissions taken up by land, (g) Ocean  
1021 uptake since 1850, (h) Fraction of cumulative emissions taken up by ocean.  
1022 Note that for individual models the ocean uptake fraction can be  $> 1$  if the  
1023 land uptake fraction is  $< 0$ . Data in panel (a) were smoothed using a ten-year  
1024 moving average. 53

- 1025 5 Changes in carbon inventories by the year 3000 as a function of the change in  
1026 atmospheric carbon between 1850 and 3000 for RCPs 2.6–8.5. (a) Cumulative  
1027 carbon emissions since 1850, (b) airborne fraction of cumulative emissions,  
1028 (c) land carbon uptake since 1850, (d) land uptake fraction, (e) ocean carbon  
1029 uptake since 1850, (f) ocean uptake fraction. 54
- 1030 6 Time evolution of climate variables under the pre-industrial CO<sub>2</sub>-emission  
1031 commitment simulations for four RCP scenarios: (a) Diagnosed cumulative  
1032 CO<sub>2</sub> emissions since 1850, (b) atmospheric CO<sub>2</sub>, (c) Surface air temperature  
1033 change, (d) Ocean thermal expansion. Anomalies are relative to 1986–2005.  
1034 Shown are the model ensemble averages (thick solid lines), the ranges spanned  
1035 by all models (shaded domains, delimited by thin solid lines), and the range  
1036 in the year 3000 (vertical bars on right hand side). Data were smoothed using  
1037 a ten-year moving average. 55
- 1038 7 RCP2.6 pre-industrial CO<sub>2</sub>-emission commitment simulations. (a) Cumula-  
1039 tive CO<sub>2</sub> emissions since 1850, (b) Atmospheric CO<sub>2</sub>, (c) Surface air temper-  
1040 ature change, (d) Ocean thermal expansion. Anomalies in panels (c) and (d)  
1041 are relative to 1986–2005. Data in panel (c) were smoothed using a ten-year  
1042 moving average. Note that the response of the UMD model differs from that  
1043 of other models due to slightly positive CO<sub>2</sub> emissions after year 2300. 56
- 1044 8 Pre-industrial CO<sub>2</sub>-emission simulations for RCPs 2.6–8.5. (a) Atmospheric  
1045 CO<sub>2</sub> in year 3000 as a fraction of atmospheric CO<sub>2</sub> in year 2300 (corresponding  
1046 to peak atmospheric CO<sub>2</sub> in RCPs 4.5–8.5), (b) Warming in year 3000 as  
1047 a fraction of warming in year 2300 (corresponding approximately to peak  
1048 warming in RCPs 4.5–8.5). Results are shown as a function of the peak  
1049 atmospheric CO<sub>2</sub> concentration in each RCP, which is the same for all models. 57

- 1050 9 Time evolution of climate variables under the pre-industrial emission commit-  
1051 ment simulations for four RCP scenarios: (a) atmospheric CO<sub>2</sub>, (b) Surface  
1052 air temperature change, (c) Ocean thermal expansion. Anomalies are relative  
1053 to 1986–2005. Shown are the model ensemble averages (thick solid lines), the  
1054 ranges spanned by all models (shaded domains, delimited by thin solid lines),  
1055 and the range in the year 3000 (vertical bars on right hand side). Data were  
1056 smoothed using a ten-year moving average. 58
- 1057 10 Time evolution of climate variables for constant-CO<sub>2</sub>-emission commitment  
1058 simulations under four RCP scenarios: (a) Diagnosed CO<sub>2</sub> emissions, (b)  
1059 atmospheric CO<sub>2</sub>, (c) Surface air temperature change, (d) Ocean thermal  
1060 expansion. Anomalies in panels (c) and (d) are relative to 1986–2005. Shown  
1061 are the model ensemble averages (thick solid lines), the ranges spanned by  
1062 all models (shaded domains, delimited by thin solid lines), and the range in  
1063 the year 3000 (vertical bars on right hand side). Data were smoothed using a  
1064 ten-year moving average. 59
- 1065 11 Time evolution of climate variables for reversibility simulations with atmo-  
1066 spheric CO<sub>2</sub> after year 3000 decreasing to pre-industrial levels over 100 years:  
1067 (a) Atmospheric CO<sub>2</sub>, (b) Surface air temperature change, (c) Ocean ther-  
1068 mal expansion, (d) Atlantic overturning index (maximum of the overturning  
1069 streamfunction in the North Atlantic). Anomalies in panels (b) and (c) are  
1070 relative to pre-industrial (1851–1860). Shown are the model ensemble aver-  
1071 ages (thick solid lines), the ranges spanned by all models (shaded domains,  
1072 delimited by thin solid lines), and the range in the year 3000 (vertical bars on  
1073 right hand side). Data were smoothed using a ten-year moving average. 60

1074 12 Time evolution of climate variables for reversibility simulations with atmo-  
1075 spheric CO<sub>2</sub> after year 3000 decreasing to pre-industrial levels over 1000 years:  
1076 (a) Atmospheric CO<sub>2</sub>, (b) Surface air temperature change, (c) Ocean thermal  
1077 expansion, (d) Atlantic meridional overturning index Atlantic overturning  
1078 index (maximum of the overturning streamfunction in the North Atlantic).  
1079 Anomalies in panels (b) and (c) are relative to pre-industrial (1851–1860).  
1080 Shown are the model ensemble averages (thick solid lines), the ranges spanned  
1081 by all models (shaded domains, delimited by thin solid lines), and the range  
1082 in the year 3000 (vertical bars on right hand side). Data were smoothed using  
1083 a ten-year moving average. 61

1084 13 Time evolution of climate variables for reversibility simulations with atmo-  
1085 spheric CO<sub>2</sub> after year 3000 evolving freely (zero emissions). These experi-  
1086 ments were performed by EMICs with an interactive carbon cycle only: (a)  
1087 Atmospheric CO<sub>2</sub>, (b) Surface air temperature change, (c) Ocean thermal ex-  
1088 pansion, (d) Atlantic overturning index (maximum of the overturning stream-  
1089 function in the North Atlantic). Anomalies in panels (b) and (c) are relative  
1090 to pre-industrial (1851–1860). Shown are the model ensemble averages (thick  
1091 solid lines), the ranges spanned by all models (shaded domains, delimited by  
1092 thin solid lines), and the range in the year 3000 (vertical bars on right hand  
1093 side). Data were smoothed using a ten-year moving average. 62

1094 14 Diagnosed CO<sub>2</sub> emissions for reversibility simulations with atmospheric CO<sub>2</sub>  
1095 after year 3000 decreasing to pre-industrial levels over 100 years (a), and 1000  
1096 years (b). Results are shown for seven EMICs with an interactive carbon  
1097 cycle. Shown are the model ensemble averages (thick solid lines), the ranges  
1098 spanned by all models (shaded domains, delimited by thin solid lines), and the  
1099 range in the year 3000 (vertical bars on right hand side). Note the different  
1100 vertical scales in panels (a) and (b). 63

- 1101 15 Changes in carbon inventories for the RCP4.5 reversibility simulation with  
1102 atmospheric CO<sub>2</sub> after year 3000 decreasing to pre-industrial levels over 100  
1103 years. (a) CO<sub>2</sub> emissions, (b) Cumulative CO<sub>2</sub> emissions since 1850, (c) Land  
1104 uptake since 1850, (d) Ocean uptake since 1850. Data in panel (a) were  
1105 smoothed using a ten-year moving average. 64
- 1106 16 Cumulative CO<sub>2</sub> emissions compatible with a set of long-term temperature  
1107 targets (1.5–4°C) for temperature tracking experiments with two EMICs:  
1108 UVic (dashed) and Bern3D-LPJ (solid). (a) Surface air temperature change  
1109 relative to pre-industrial (1800 for UVic, 850 for Bern3D-LPJ), (b) Cumula-  
1110 tive CO<sub>2</sub> emissions since pre-industrial. 65
- 1111 17 Cumulative CO<sub>2</sub> emissions compatible with a set of long-term temperature  
1112 targets (1.5–4°C) for EMICs with an interactive carbon cycle. Allowable  
1113 cumulative emissions are derived from the models' Climate Carbon Response  
1114 (CCR) given in Table 4 of Eby et al. (2013). Also shown are the year-2500  
1115 cumulative emissions derived from temperature tracking experiments (TTR)  
1116 with the UVic and Bern3D-LPJ EMICs (square symbols). 66

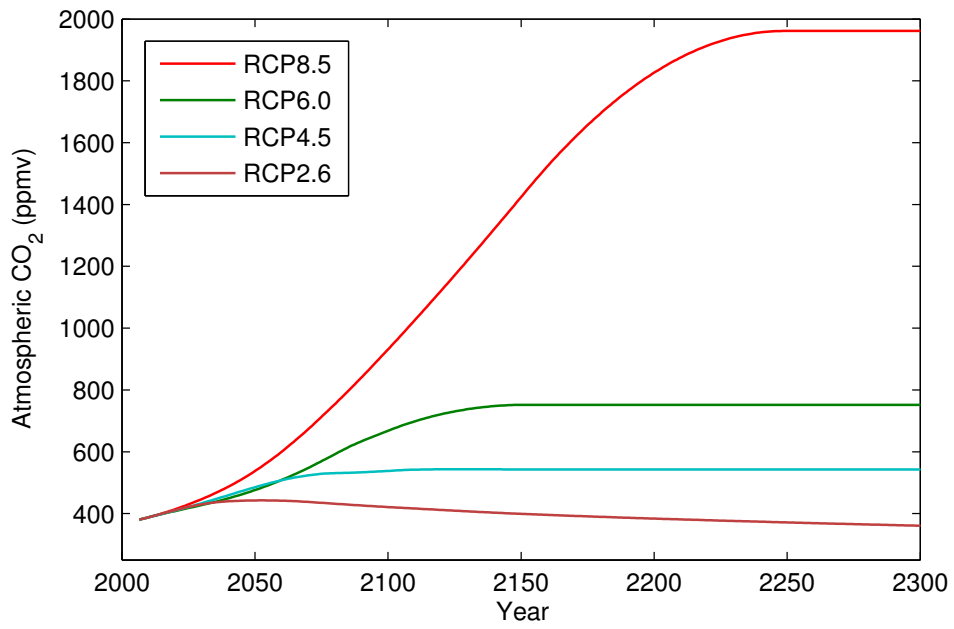


FIG. 1. Time evolution of atmospheric CO<sub>2</sub> between 2006 and 2300 for the four RCP scenarios and their extensions (RCP database version 2.0, <https://www.iiasa.ac.at/web-apps/tnt/RcpDb/>).



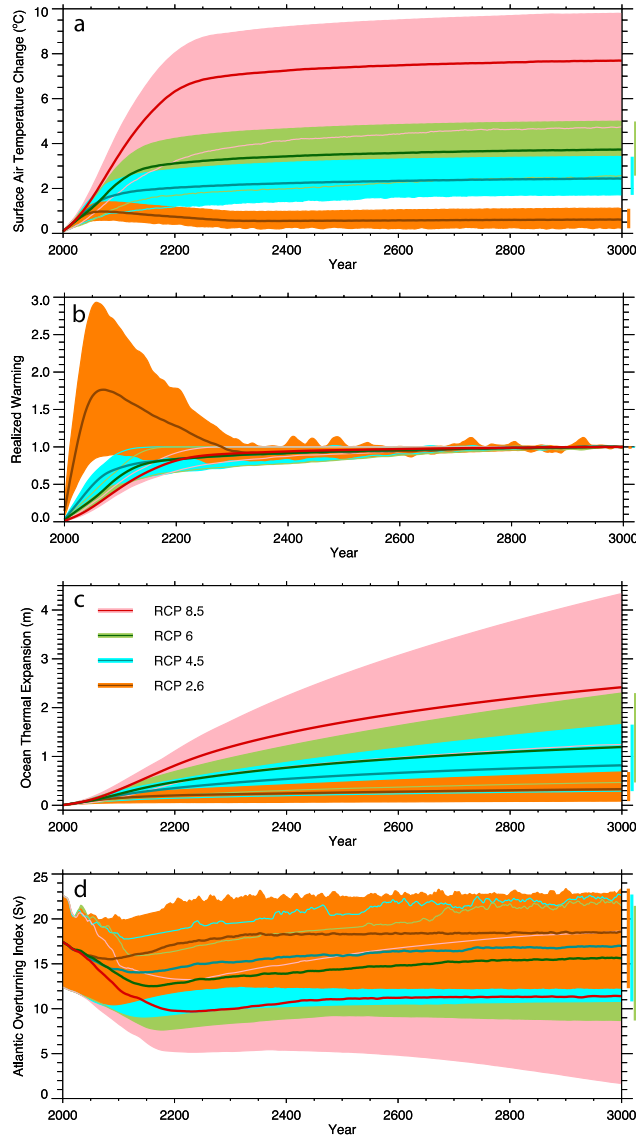


FIG. 2. Constant composition commitment. Time evolution of physical climate variables for four RCP scenarios: (a) Surface air temperature change, (b) Fraction of realized warming (calculated as the ratio of warming at any time to the warming averaged over 2981–3000), (c) Ocean thermal expansion, (d) Atlantic overturning index, defined as the maximum value of the overturning streamfunction in the North Atlantic. Anomalies are relative to 1986–2005. Shown are the model ensemble averages (thick solid lines), the ranges spanned by all models (shaded domains, delimited by thin solid lines), and the range in the year 3000 (vertical bars on right hand side). Data were smoothed using a ten-year moving average.

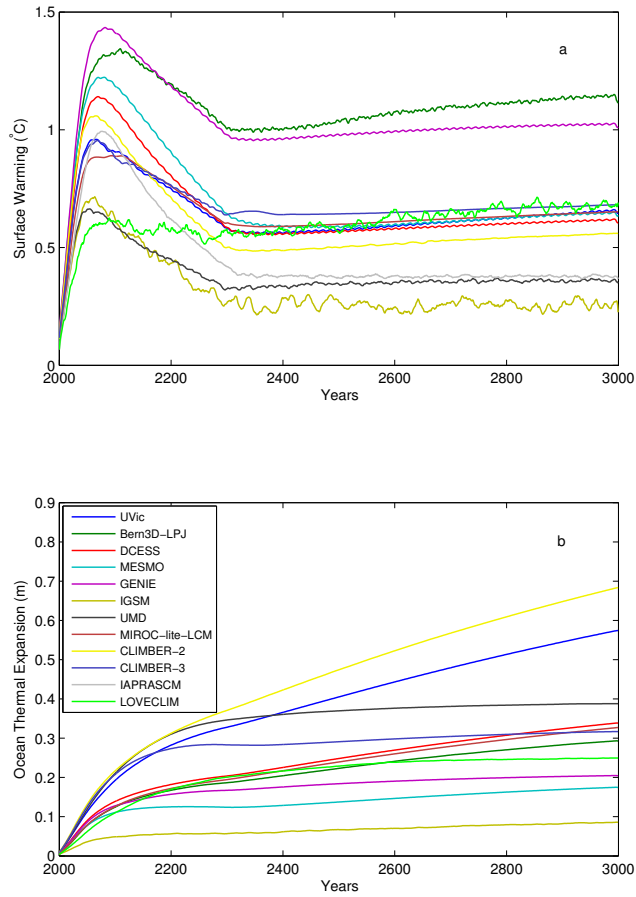


FIG. 3. RCP2.6 constant composition commitment simulations. (a) Surface air temperature change, (b) Ocean thermal expansion. Anomalies are relative to 1986–2005. Data in panel (a) were smoothed using a ten-year moving average.

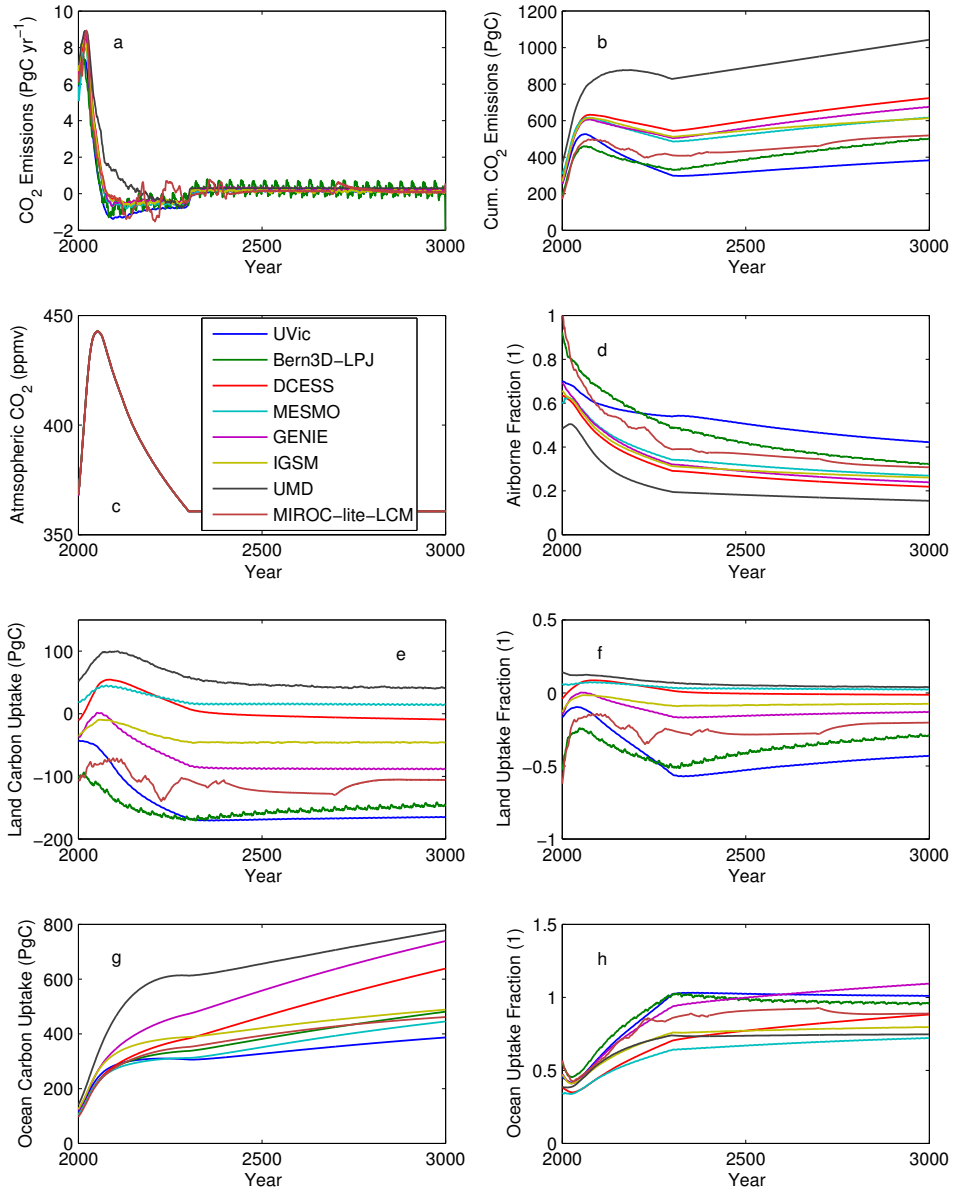


FIG. 4. Changes in carbon inventories in RCP2.6 constant composition commitment simulations for eight EMICs with an interactive carbon cycle. (a)  $\text{CO}_2$  emissions, (b) Cumulative  $\text{CO}_2$  emissions since 1850, (c) Atmospheric  $\text{CO}_2$  concentration, (d) Airborne fraction of cumulative emissions, (e) Land uptake since 1850, (f) Fraction of cumulative emissions taken up by land, (g) Ocean uptake since 1850, (h) Fraction of cumulative emissions taken up by ocean. Note that for individual models the ocean uptake fraction can be  $> 1$  if the land uptake fraction is  $< 0$ . Data in panel (a) were smoothed using a ten-year moving average.

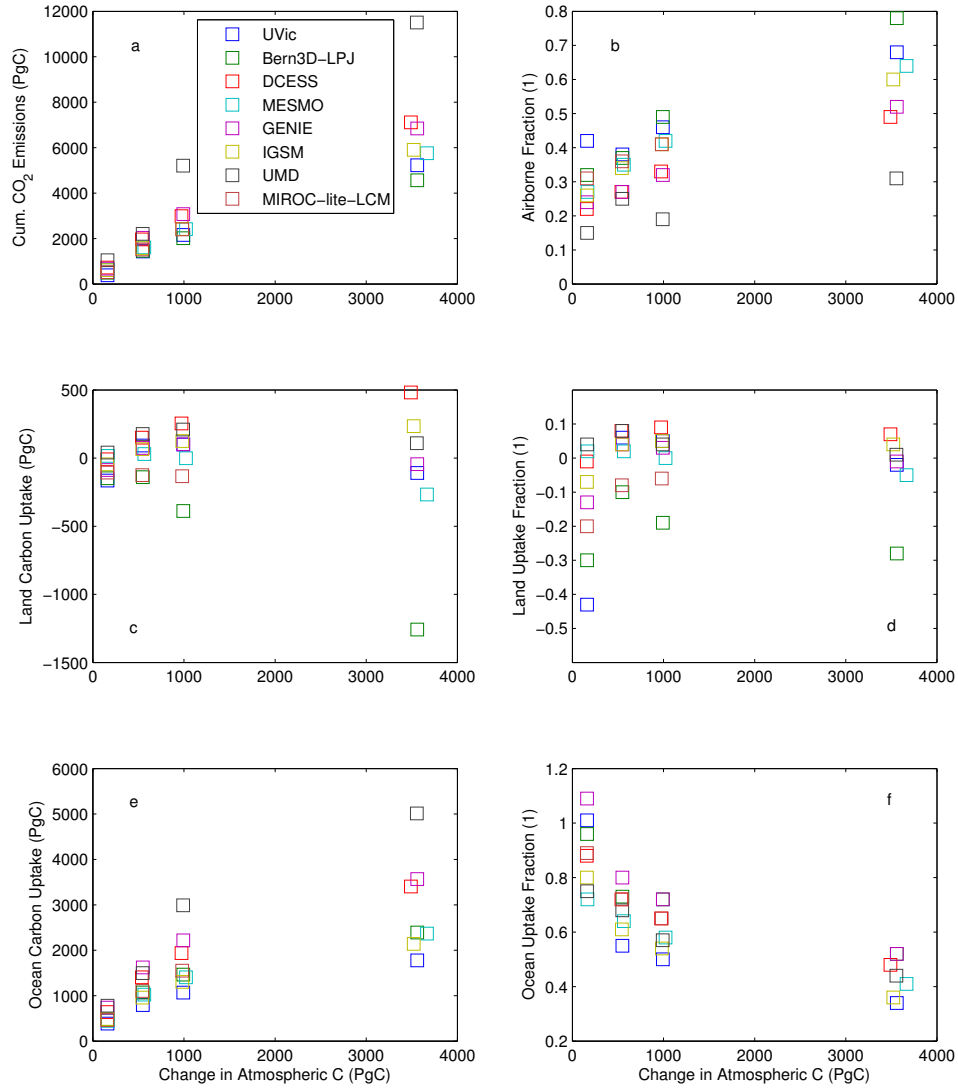


FIG. 5. Changes in carbon inventories by the year 3000 as a function of the change in atmospheric carbon between 1850 and 3000 for RCPs 2.6–8.5. (a) Cumulative carbon emissions since 1850, (b) airborne fraction of cumulative emissions, (c) land carbon uptake since 1850, (d) land uptake fraction, (e) ocean carbon uptake since 1850, (f) ocean uptake fraction.

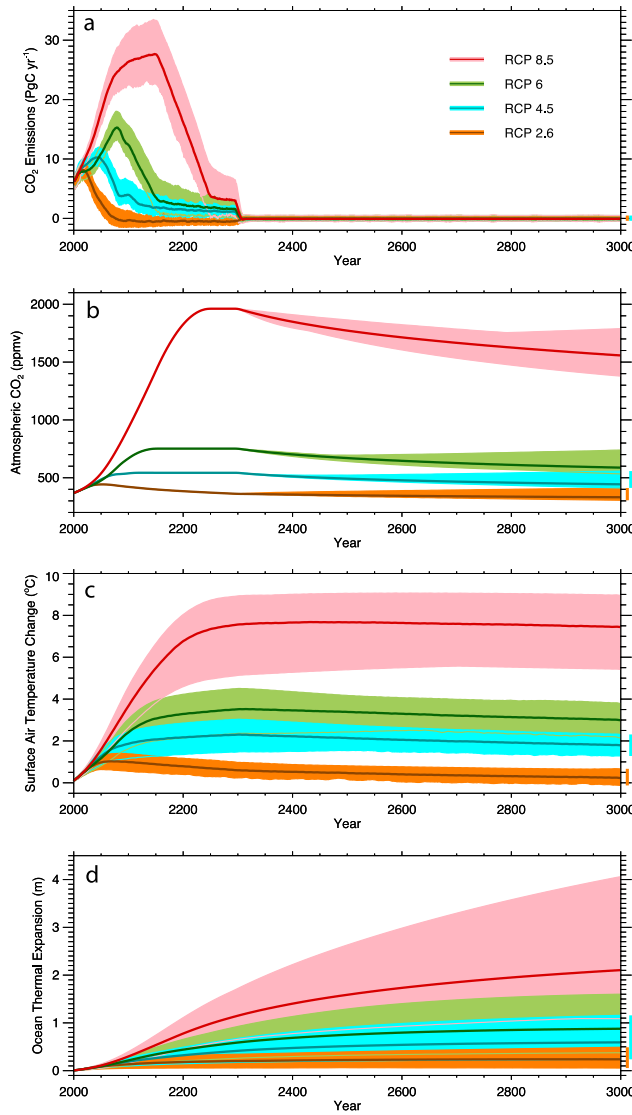


FIG. 6. Time evolution of climate variables under the pre-industrial CO<sub>2</sub>-emission commitment simulations for four RCP scenarios: (a) Diagnosed cumulative CO<sub>2</sub> emissions since 1850, (b) atmospheric CO<sub>2</sub>, (c) Surface air temperature change, (d) Ocean thermal expansion. Anomalies are relative to 1986–2005. Shown are the model ensemble averages (thick solid lines), the ranges spanned by all models (shaded domains, delimited by thin solid lines), and the range in the year 3000 (vertical bars on right hand side). Data were smoothed using a ten-year moving average.

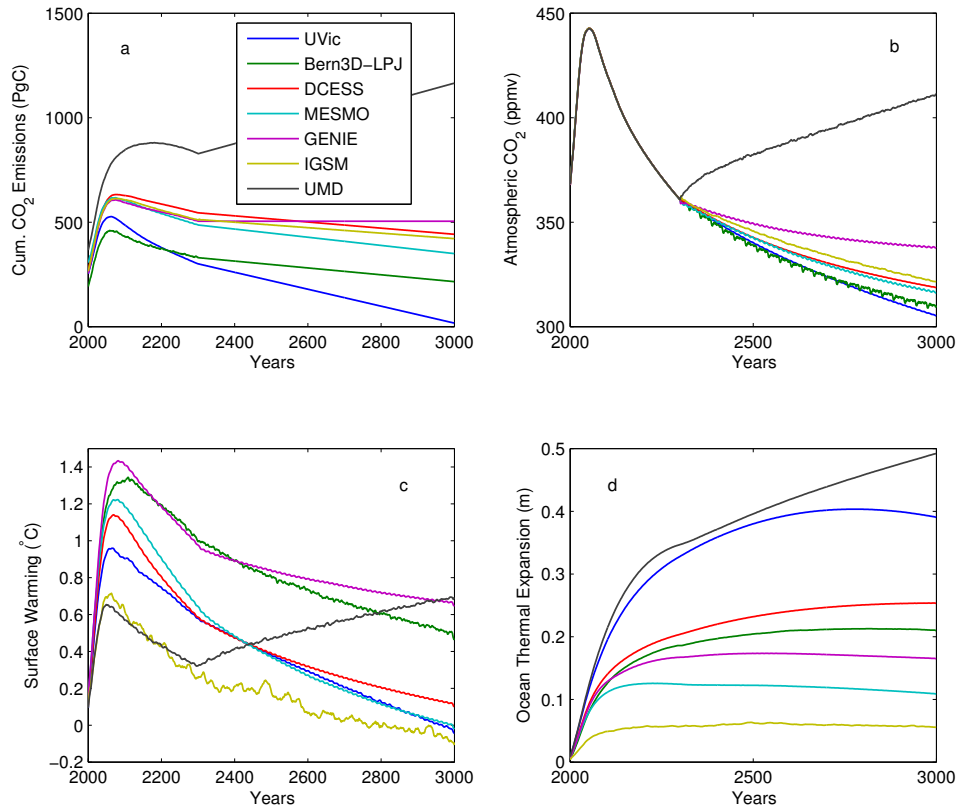


FIG. 7. RCP2.6 pre-industrial CO<sub>2</sub>-emission commitment simulations. (a) Cumulative CO<sub>2</sub> emissions since 1850, (b) Atmospheric CO<sub>2</sub>, (c) Surface air temperature change, (d) Ocean thermal expansion. Anomalies in panels (c) and (d) are relative to 1986–2005. Data in panel (c) were smoothed using a ten-year moving average. Note that the response of the UMD model differs from that of other models due to slightly positive CO<sub>2</sub> emissions after year 2300.

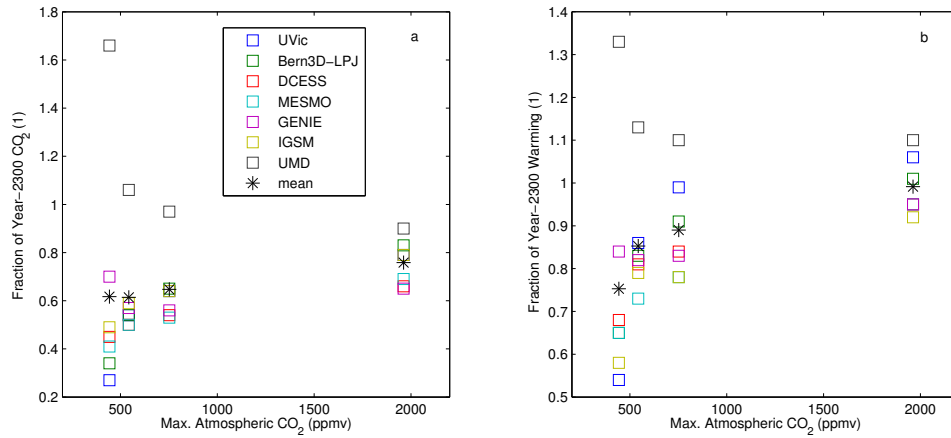


FIG. 8. Pre-industrial CO<sub>2</sub>-emission simulations for RCPs 2.6–8.5. (a) Atmospheric CO<sub>2</sub> in year 3000 as a fraction of atmospheric CO<sub>2</sub> in year 2300 (corresponding to peak atmospheric CO<sub>2</sub> in RCPs 4.5–8.5), (b) Warming in year 3000 as a fraction of warming in year 2300 (corresponding approximately to peak warming in RCPs 4.5–8.5). Results are shown as a function of the peak atmospheric CO<sub>2</sub> concentration in each RCP, which is the same for all models.

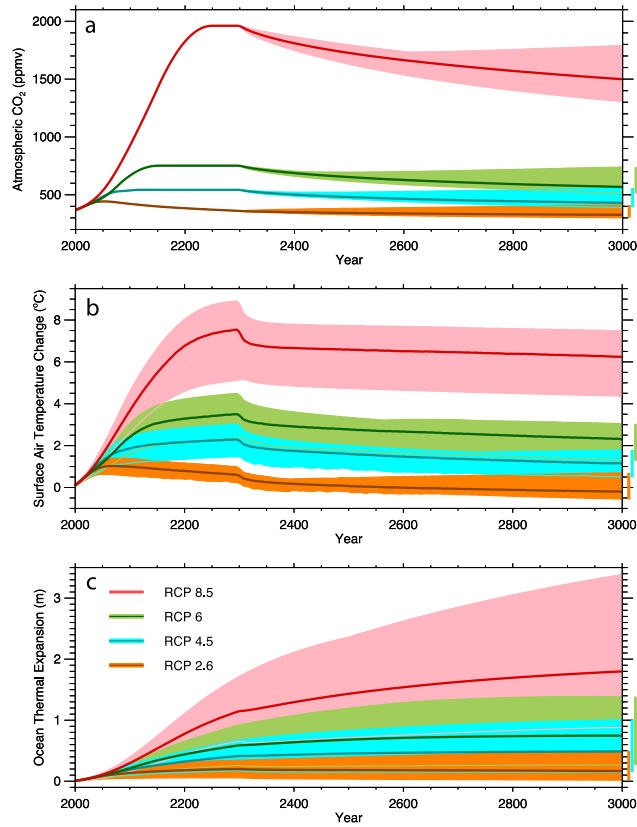


FIG. 9. Time evolution of climate variables under the pre-industrial emission commitment simulations for four RCP scenarios: (a) atmospheric CO<sub>2</sub>, (b) Surface air temperature change, (c) Ocean thermal expansion. Anomalies are relative to 1986–2005. Shown are the model ensemble averages (thick solid lines), the ranges spanned by all models (shaded domains, delimited by thin solid lines), and the range in the year 3000 (vertical bars on right hand side). Data were smoothed using a ten-year moving average.



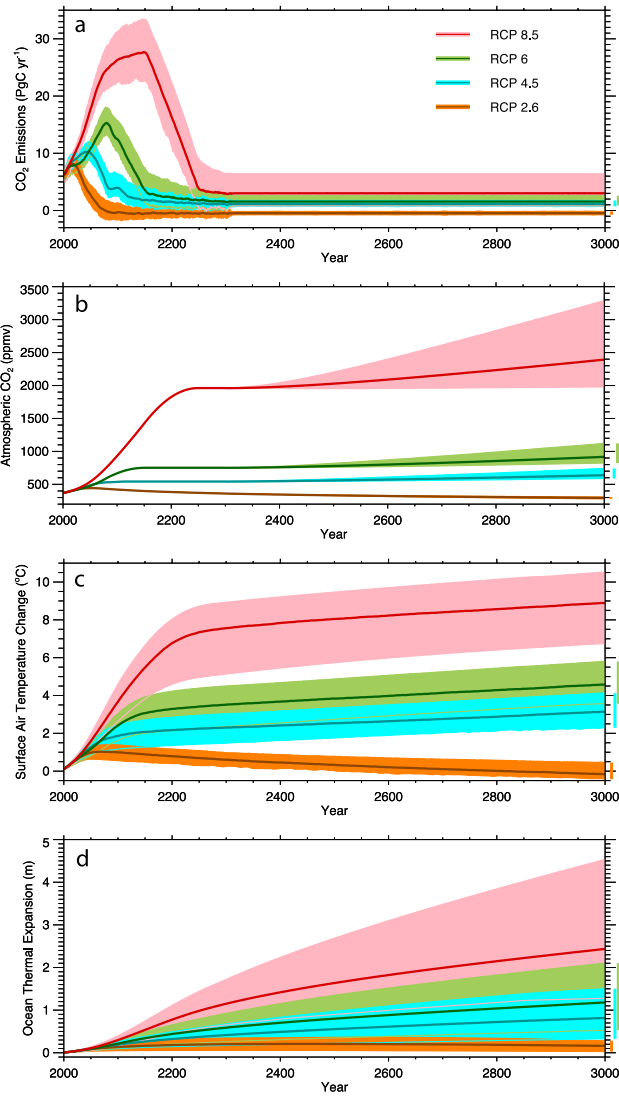


FIG. 10. Time evolution of climate variables for constant- $\text{CO}_2$ -emission commitment simulations under four RCP scenarios: (a) Diagnosed  $\text{CO}_2$  emissions, (b) atmospheric  $\text{CO}_2$ , (c) Surface air temperature change, (d) Ocean thermal expansion. Anomalies in panels (c) and (d) are relative to 1986–2005. Shown are the model ensemble averages (thick solid lines), the ranges spanned by all models (shaded domains, delimited by thin solid lines), and the range in the year 3000 (vertical bars on right hand side). Data were smoothed using a ten-year moving average.

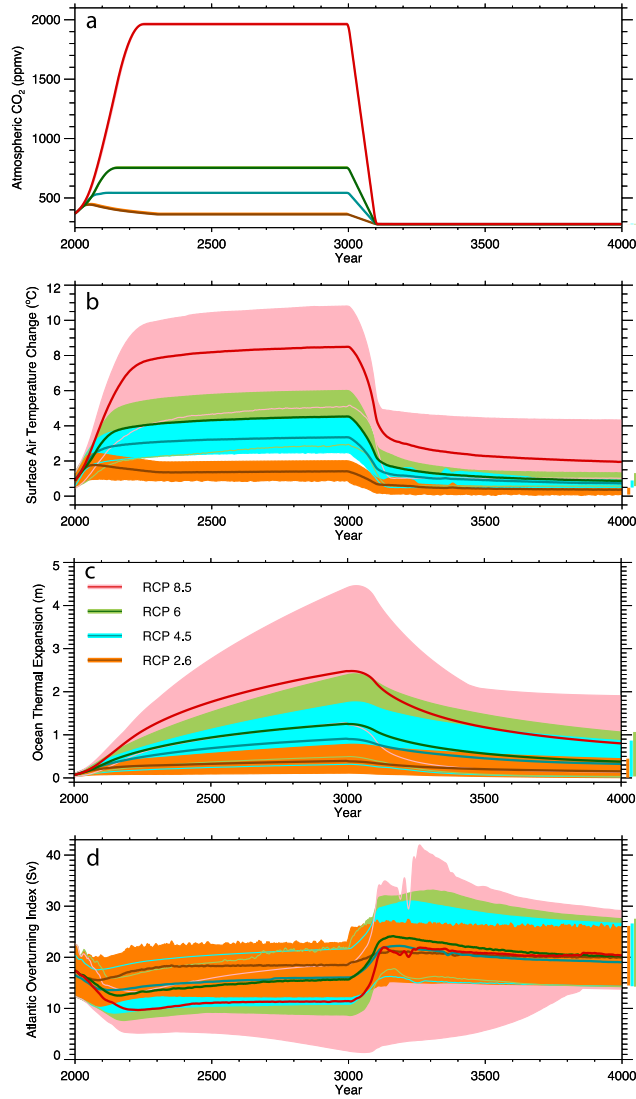


FIG. 11. Time evolution of climate variables for reversibility simulations with atmospheric  $\text{CO}_2$  after year 3000 decreasing to pre-industrial levels over 100 years: (a) Atmospheric  $\text{CO}_2$ , (b) Surface air temperature change, (c) Ocean thermal expansion, (d) Atlantic overturning index (maximum of the overturning streamfunction in the North Atlantic). Anomalies in panels (b) and (c) are relative to pre-industrial (1851–1860). Shown are the model ensemble averages (thick solid lines), the ranges spanned by all models (shaded domains, delimited by thin solid lines), and the range in the year 3000 (vertical bars on right hand side). Data were smoothed using a ten-year moving average.

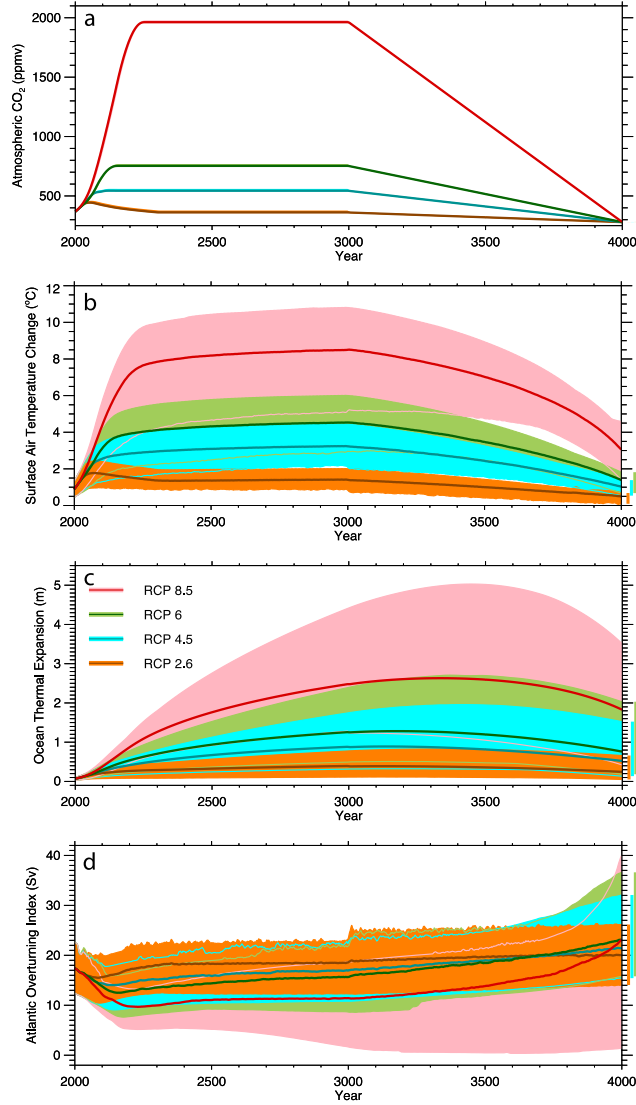


FIG. 12. Time evolution of climate variables for reversibility simulations with atmospheric CO<sub>2</sub> after year 3000 decreasing to pre-industrial levels over 1000 years: (a) Atmospheric CO<sub>2</sub>, (b) Surface air temperature change, (c) Ocean thermal expansion, (d) Atlantic meridional overturning index Atlantic overturning index (maximum of the overturning streamfunction in the North Atlantic). Anomalies in panels (b) and (c) are relative to pre-industrial (1851–1860). Shown are the model ensemble averages (thick solid lines), the ranges spanned by all models (shaded domains, delimited by thin solid lines), and the range in the year 3000 (vertical bars on right hand side). Data were smoothed using a ten-year moving average.

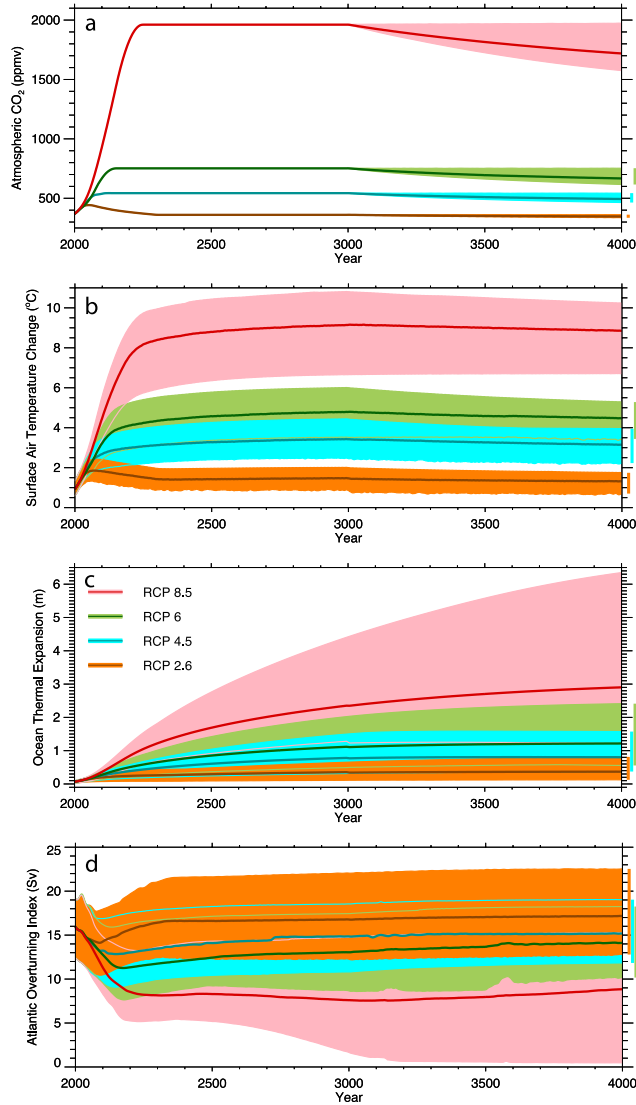


FIG. 13. Time evolution of climate variables for reversibility simulations with atmospheric  $\text{CO}_2$  after year 3000 evolving freely (zero emissions). These experiments were performed by EMICs with an interactive carbon cycle only: (a) Atmospheric  $\text{CO}_2$ , (b) Surface air temperature change, (c) Ocean thermal expansion, (d) Atlantic overturning index (maximum of the overturning streamfunction in the North Atlantic). Anomalies in panels (b) and (c) are relative to pre-industrial (1851–1860). Shown are the model ensemble averages (thick solid lines), the ranges spanned by all models (shaded domains, delimited by thin solid lines), and the range in the year 3000 (vertical bars on right hand side). Data were smoothed using a ten-year moving average.

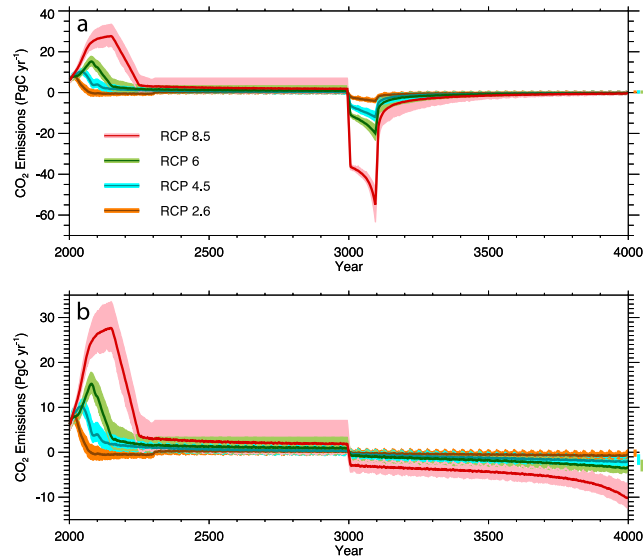


FIG. 14. Diagnosed CO<sub>2</sub> emissions for reversibility simulations with atmospheric CO<sub>2</sub> after year 3000 decreasing to pre-industrial levels over 100 years (a), and 1000 years (b). Results are shown for seven EMICs with an interactive carbon cycle. Shown are the model ensemble averages (thick solid lines), the ranges spanned by all models (shaded domains, delimited by thin solid lines), and the range in the year 3000 (vertical bars on right hand side). Note the different vertical scales in panels (a) and (b).

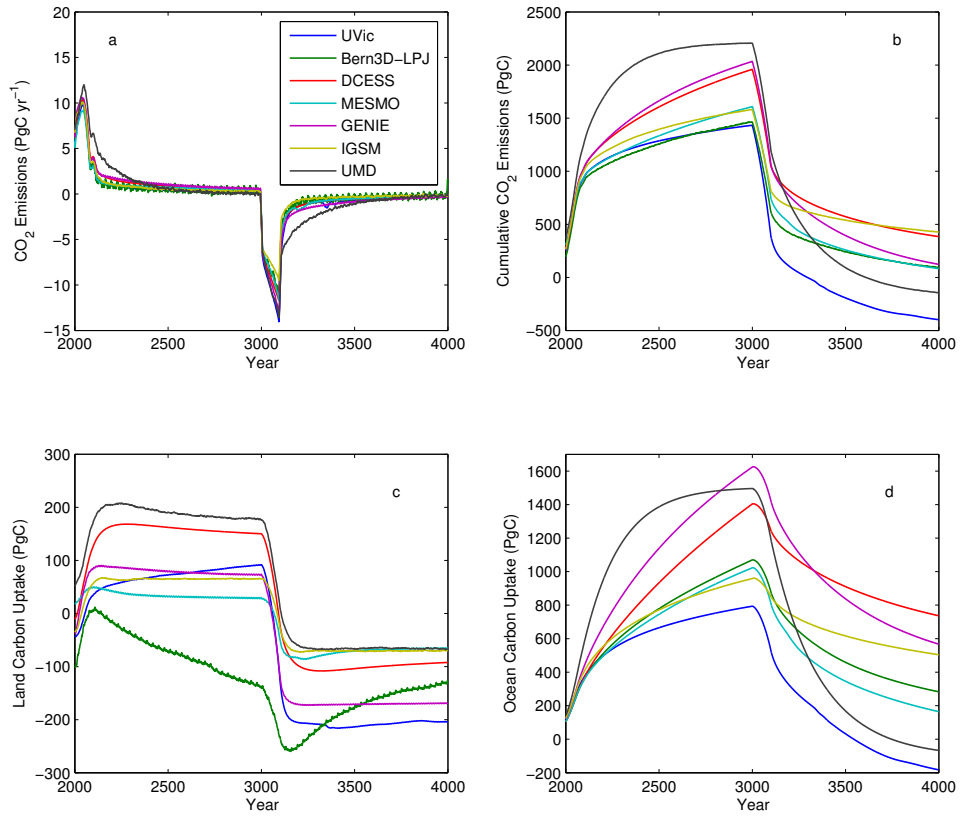


FIG. 15. Changes in carbon inventories for the RCP4.5 reversibility simulation with atmospheric CO<sub>2</sub> after year 3000 decreasing to pre-industrial levels over 100 years. (a) CO<sub>2</sub> emissions, (b) Cumulative CO<sub>2</sub> emissions since 1850, (c) Land uptake since 1850, (d) Ocean uptake since 1850. Data in panel (a) were smoothed using a ten-year moving average.

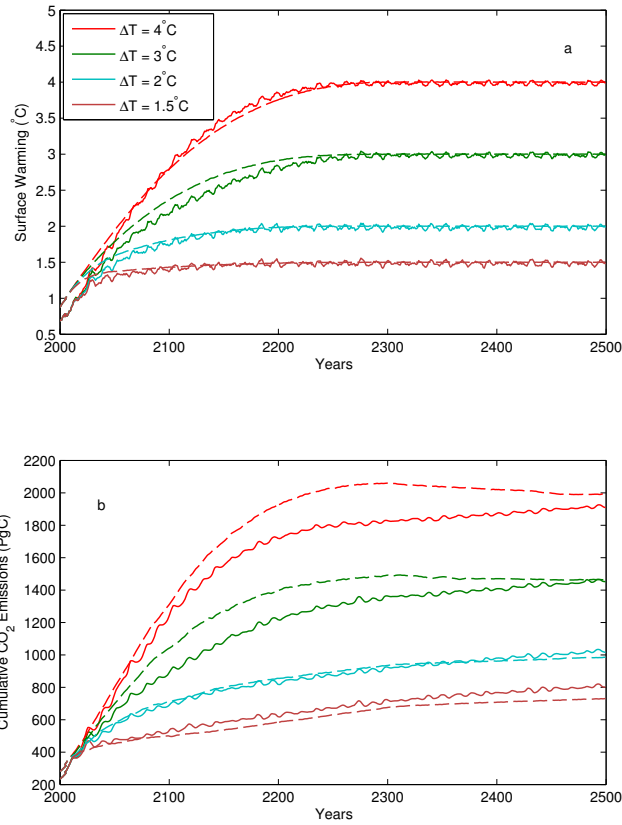


FIG. 16. Cumulative CO<sub>2</sub> emissions compatible with a set of long-term temperature targets (1.5–4°C) for temperature tracking experiments with two EMICs: UVic (dashed) and Bern3D-LPJ (solid). (a) Surface air temperature change relative to pre-industrial (1800 for UVic, 850 for Bern3D-LPJ), (b) Cumulative CO<sub>2</sub> emissions since pre-industrial.

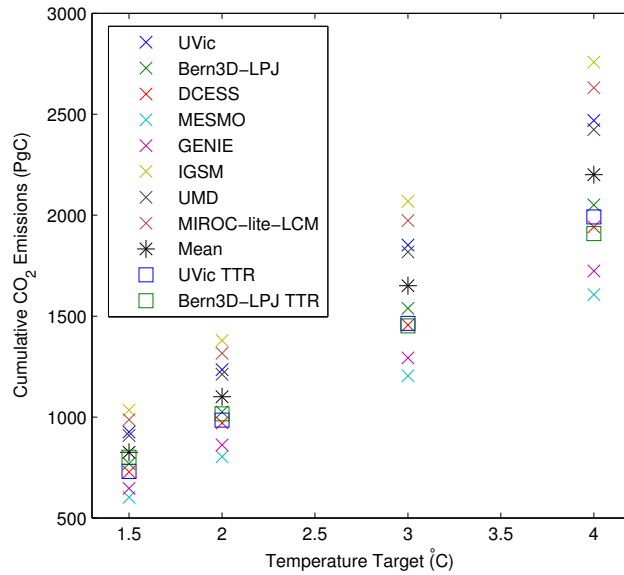


FIG. 17. Cumulative CO<sub>2</sub> emissions compatible with a set of long-term temperature targets (1.5–4°C) for EMICs with an interactive carbon cycle. Allowable cumulative emissions are derived from the models’ Climate Carbon Response (CCR) given in Table 4 of Eby et al. (2013). Also shown are the year-2500 cumulative emissions derived from temperature tracking experiments (TTR) with the UVic and Bern3D-LPJ EMICs (square symbols).